

Late Cenozoic deformation of the Kura fold-thrust belt, southern Greater Caucasus

A.M. Forte^{1,†}, E. Cowgill¹, T. Bernardin², O. Kreylos², and B. Hamann²

¹*Department of Geology, University of California, Davis, Davis, California 95616, USA*

²*Institute of Data Analysis and Visualization, Department of Computer Sciences, University of California, Davis, Davis, California 95616, USA*

ABSTRACT

Although the geometry and kinematics of the first-order structures accommodating Arabia-Eurasia convergence are relatively well known in Turkey and Iran, major shortening structures remain poorly understood within the central portion of the collision zone, in eastern Anatolia and the Caucasus. New remotely sensed neotectonic mapping, synthesis of regional geologic and stratigraphic data, and balanced cross sections suggest that the Kura fold-thrust belt has accommodated the majority of Arabia-Eurasia convergence since the early Pliocene between the longitudes of ~45°E and ~49°E. This belt lies southeast of the N80°W-striking Greater Caucasus Mountains and forms an eastward-narrowing band of elevated topography that roughly parallels the range front for ~400 km along strike. The belt is separated from the Greater Caucasus to the north by the 10- to 25-km-wide Alazani Basin and comprises a series of predominantly south-verging folds deforming Eocene-Quaternary flysch and molasse. To document structural geometries within the Kura fold-thrust belt, we have used the Real-time Interactive Mapping System (RIMS) software to analyze Advanced Spaceborne Thermal Emission and Reflection Radiometer (ASTER), visible to near-infrared (VNIR), and digital elevation model (DEM) data. This neotectonic mapping indicates an along-strike, eastward decrease in both structural complexity and the degree to which deformed geomorphic surfaces are dissected. Existing geologic maps indicate a corresponding eastward decrease in the depth of exposure. By integrating the structural geometries determined in our analysis of remote-sensing data with existing geologic data, we have constructed two balanced cross sections, which suggest these

systematic along-strike variations result from a west-to-east decrease in total shortening within the Kura fold-thrust belt. We interpret this variable shortening to stem from eastward propagation of the Kura fold-thrust belt. Comparison of our preliminary total shortening estimates with those predicted by current plate motions suggest that the Kura fold-thrust belt has accommodated ~30%–40% (~25 km) of total Arabia-Eurasia convergence since 5 Ma, and thus forms a first-order structural system within the central portion of the collision zone.

INTRODUCTION

Much of our current understanding of how convergent deformation is accommodated within continents has come from intensive study of the Alpine-Himalayan orogenic system, which stretches from western Europe to eastern China. Previous work within this system has largely focused on the two end segments of the mountain chain, the Alps at the western end and the Himalaya and Tibetan Plateau to the east. In comparison, the central part of the collision zone, between Arabia and Eurasia, has received less attention, although it has produced both the Greater and Lesser Caucasus Mountains and the Turkish-Iranian Plateau. Both the Alps and Himalayas are essentially “middle-aged” in the terms of orogenic systems, and as such, record orogenic processes that are active within mature mountain ranges. However, the early stages of deformation have been overprinted in both belts (Axen et al., 2001). Alternatively, the Arabia-Eurasia collision is in a much earlier stage of development, and hence provides a unique and, as of yet, largely untapped resource for understanding the dynamics and evolution of young continent-continent collisions.

Late Mesozoic to Cenozoic closure of the Neotethys Ocean and subsequent collision of the Arabian and Eurasian continents has produced a zone of deformation within the Alpine-

Himalayan belt that extends over 2500 km along strike. Estimates for the timing of collision between Arabia and Eurasia are poorly constrained and include early Paleocene (Berberian and King, 1981), Eocene (Hempton, 1987), early Miocene (Robertson, 2000), mid-Miocene (Dewey et al., 1986), late Miocene (McQuarrie et al., 2003), and early Pliocene (Philip et al., 1989). Increasingly it has been recognized that the wide variation in reported ages of collision may result from both diachronous timing of collision along strike and numerous small collisional events occurring throughout the Cenozoic, but the current best estimates suggest that continental collision began ca. 35 Ma (Allen and Armstrong, 2008) and that consumption of Neotethys was complete by ca. 11 Ma (e.g., Keskin, 2003; Şengör et al., 2003; Hafkenscheid et al., 2006). Although a major reorganization of the collision zone occurred at ca. 5 Ma, it appears that current plate motions and boundaries can be extrapolated back to this time (e.g., Westaway, 1994; McQuarrie et al., 2003; Allen et al., 2004).

The first-order structural systems accommodating northward movement of Arabia with respect to Eurasia since 5 Ma are relatively well understood in the western and eastern thirds of the collision. West of 41°E, convergence has been absorbed by the westward expulsion of Anatolia along the conjugate right-slip North Anatolian and left-slip East Anatolian faults (McKenzie, 1972). East of 48°E, oblique convergence has been accommodated by NE-SW thrusting in the Zagros, both NE-SW-directed thrusting and dextral movement along the Main Recent Fault (Talebian and Jackson, 2002), and N-S shortening across the Alborz range (Axen et al., 2001; Guest et al., 2006) and Apsheron Sill (Allen et al., 2002). In contrast, the location, geometry, and kinematics of the first-order structural systems in the central third of the collision (41°E to 48°E) remain unclear (Fig. 1A).

The central portion of the collision zone lies between the Black and Caspian Seas, and contains

[†]E-mail: amforte@ucdavis.edu

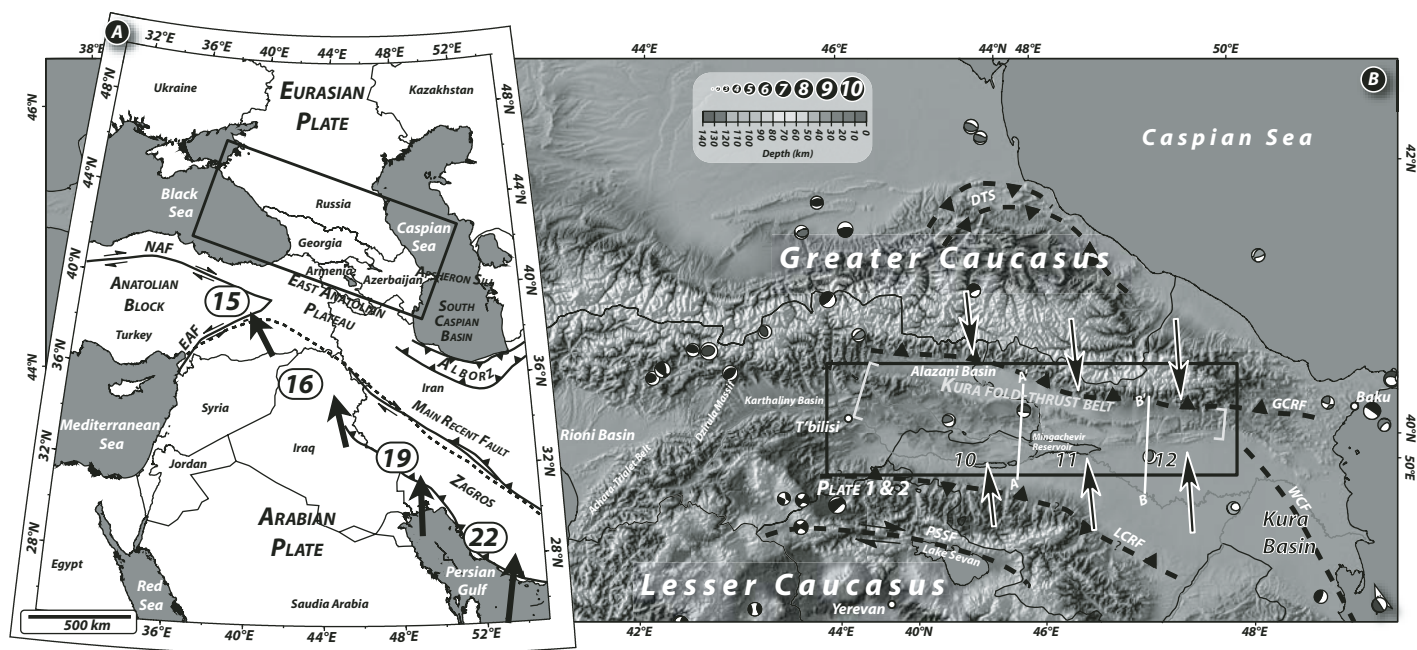


Figure 1. Maps showing Arabia-Eurasia kinematics, major structures, and location of the Kura fold-thrust belt. (A) Overview of the Arabia-Eurasia collision zone. Arrows with numbers indicating rates (mm/a) show motion of Arabian plate relative to stable Eurasia as computed using REVEL 2000 velocity model (Sella et al., 2002) and the UNAVCO plate motion calculator at http://sps.unavco.org/crustal_motion/dxdt/nrncalc/. Solid lines show first-order structures in the western and eastern thirds of the collision zone (NAF—North Anatolian fault; EAF—East Anatolian fault). Dotted black line represents approximate location of the Bitlis suture, and black box outlines the extent of Figure 1B. (B) Shaded relief map of the Caucasus region and Kura Basin. White brackets frame Kura fold-thrust belt. Pairs of opposing black arrows indicate current shortening rates across the southeastern margin of the Greater Caucasus derived from a global positioning system (GPS) block model (Reilinger et al., 2006). Black box outlines the boundaries of neotectonic (Plate 1) and geologic (Plate 2) maps, and lines A–A' and B–B' represent the lines of section illustrated in Figures 8 and 9, respectively. Focal mechanisms of major earthquakes from the global Centroid Moment Tensor (CMT) catalog (<http://www.globalcmt.org>). Major structures discussed in the text appear in black (DTS—Dagestan Thrust System, GCRF—Greater Caucasus Range-Front Fault system, WCF—West Caspian Fault, LCRF—Lesser Caucasus Range-Front Fault, PSSF—Pambak-Sevan-Sunik Fault). The locations of the GCRF, LCRF, and PSSF come from Koçyiğit et al. (2001), the WCF from Allen et al. (2003), and the DTS from Philip et al. (1989). It should be noted that as described in the text the exact location, kinematics, and activity of these structures are disputed. Base hillshade image generated from Shuttle Radar Topographic Mission (SRTM) 90-m digital elevation model (DEM). A color version of this figure is available in the GSA Data Repository.

both the East Anatolian Plateau and the Greater and Lesser Caucasus Mountains (Fig. 1). In this area, both local (Reilinger et al., 2006) and global (Sella et al., 2002) plate motions derived from global positioning system (GPS) measurements indicate Arabia currently moves at 15–16 mm/a toward N10°W relative to stable Eurasia, which is oblique to the N80°W strike of this portion of the collision zone (Fig. 1A).

It has long been argued that this oblique motion is partitioned between slip on conjugate sets of NW-striking dextral and NE-striking sinistral strike-slip faults in the East Anatolian Plateau and range-perpendicular shortening within the ~N80°W-striking Greater Caucasus (e.g., Jackson, 1992; Reilinger et al., 1997; McClusky et al., 2000; Vernant et al., 2004; Dhont and Chorowicz, 2006). A series of north-dipping thrusts (Koçyiğit et al., 2001) defines the south-

ern front of the Greater Caucasus range and are commonly interpreted as the most important shortening structural system in the Caucasus region (e.g., Reilinger et al., 2006). Recent GPS surveys indicate that most of the East Anatolian Plateau and the Lesser Caucasus appears to behave rigidly, with <1–2 mm/a of internal deformation (Reilinger et al., 2006), implying that 8–14 mm/a of Arabia-Eurasia convergence occurs north of the Lesser Caucasus, between the Kura Basin and the Greater Caucasus (Fig. 1B, Reilinger et al., 2006; Allmendinger et al., 2007). However, the density of GPS stations is insufficient to resolve the locations of the major structures along which this NE-SW-directed shortening occurs.

Previous workers have suggested that shortening in the Greater Caucasus region is localized along the southern range front (Philip et al.,

1989; Allen et al., 2004), based on clusters of seismicity with focal mechanisms indicating south-directed thrusting (Jackson, 1992). However, this pattern of seismicity may not accurately reflect the location and kinematics of the first-order structures in this region, because coseismic deformation accounts for only 10%–20% of the deformation in the Caucasus region (e.g., Westaway, 1990; Jackson, 1992; Tan and Taymaz, 2006). Allen et al. (2003) hypothesized that deformation within the Greater Caucasus has propagated both eastward, into the South Caspian, and into both the northern and southern forelands flanking the range.

To address this problem, we used remote sensing techniques and previously published bedrock geology and stratigraphic studies to investigate the neotectonic geology of the Kura fold-thrust belt, which is an elongate range of

topography that lies southeast of the Greater Caucasus and roughly parallels the Greater Caucasus range front for ~400 km along strike. This chain of ridges and valleys lies within Azerbaijan and eastern Georgia and separates the Alazani and Kura basins to the north and south, respectively (Fig. 1B). Here we document structural geometries within the Kura fold-thrust belt by using new software tools (Bernardin et al., 2006) to analyze remotely sensed multispectral and digital elevation data. Together with previous results, our work suggests that the Kura fold-thrust belt has accommodated ~30%–45% of total Arabia-Eurasia convergence since 5 Ma at these longitudes, and appears to have initiated diachronously along strike due to eastward propagation of deformation.

We begin our summary of the Kura fold-thrust belt with a brief discussion of the geologic history of the Kura Basin and surrounding regions since 5 Ma. We then describe our neotectonic observations, which indicate that the Kura fold-thrust belt comprises a series of actively growing folds with axes trending roughly parallel to the Greater Caucasus range front. To understand the style of shortening within this fold-thrust belt, we then integrate the structural geometries determined in our neotectonic mapping with a new compilation of geologic and stratigraphic observations to produce a pair of balanced cross sections, which we use to estimate the magnitude and age of shortening within the fold-thrust belt. Finally we conclude by discussing the implications of these results on the kinematic evolution of the central Arabia-Eurasia collision since 5 Ma (early Pliocene).

TECTONIC SETTING

Kura and Alazani Basins

The Kura fold-thrust belt defines the northern edge of the Kura Basin, which separates the Greater and Lesser Caucasus Mountains to the north and south, respectively, and which has a long axis that trends roughly parallel to the strike of the Greater Caucasus (Fig. 1B). Although the topographic range herein referred to as the Kura fold-thrust belt has previously been called the Transcaucasus (Koçyiğit et al., 2001), we do not use this name because it has also been used to refer to a number of different features in the region, as reviewed by Banks et al. (1997). For example, Khain (1975) used the name “Transcaucasus” to describe the entire region separating the Greater and Lesser Caucasus ranges between the Black to the Caspian seas and including the Kura, Alazani, Rioni, and Karthaliny basins as well as the Dzirula massif (Fig. 1B). Alternatively, the term has also

been used to refer just to the Lesser Caucasus and their eastern extensions (Sobornov, 1994; Yılmaz et al., 2000) or just the Achara-Trialet belt (Fig. 1B) (Adamia et al., 1992; Golonka, 2004, 2007).

The geologic history and role of the Kura Basin within the Arabia-Eurasia collision zone remain enigmatic. The basement underlying this basin has been interpreted as a westward continuation of the oceanic crust that underlies the South Caspian basin (Zonenshain and Le Pichon, 1986). More recently, it has been suggested that much of the Kura Basin is underlain by a Jurassic to Cretaceous island arc (Nadirov et al., 1997). The total crustal thickness of the Kura Basin decreases from ~60 km along the western margin of the basin to ~45 km adjacent to the South Caspian depression (Mangino and Priestly, 1998). This decrease appears to result from the gradual eastward thinning of the lower crustal section (Mangino and Priestly, 1998), which is overlain by a relatively constant cover sequence of 5–8 km of Cenozoic sediments and ~10 km of Mesozoic crystalline and volcanic rocks (Mangino and Priestly, 1998; Ershov et al., 2003).

Koçyiğit et al. (2001) describe the Kura Basin as a flexural foreland basin. Along its western margin (~45°E), NE-SW-trending seismic sections indicate a typical foreland geometry, in which Cenozoic siliciclastic sediments are ~5–8 km thick near the Greater Caucasus range front and then gradually thin southward toward the Lesser Caucasus (Ershov et al., 2003). The smaller Alazani Basin, which is separated from the Kura Basin by the Kura fold-thrust belt (Fig. 1B), appears to be a piggy-back basin underlain by a décollement linking faults along the Greater Caucasus range front with structures in the Kura fold-thrust belt (e.g., Philip et al., 1989; Koçyiğit et al., 2001).

The sedimentary fill of the Kura Basin has been described as either molasse within an intermontane basin (Khain, 1975; Kremenetskiy et al., 1990; Tevelev and Blyumkin, 1990) or as an accretionary prism (Philip et al., 1989). The overall Cenozoic sedimentary sequence within the Kura Basin is generally equivalent to that in the South Caspian basin, although the total thickness of the Cenozoic section varies significantly, from ~5–7 km in the Kura Basin (Agabekov et al., 1976; Mangino and Priestly, 1998) to >20 km in the South Caspian Basin (Berberian, 1983). In the Kura Basin, seismic sections and well log data both indicate that strata have a regional dip of 1°–2° N and that stratal thicknesses of Plio-Pleistocene sediments increase northward, toward the Greater Caucasus range front (Agabekov et al., 1971, 1976; Ershov et al., 2003), but that thicknesses

of Pre-Pliocene sediments do not appear to vary systematically from north to south (Agabekov et al., 1976). This observation is consistent with the interpretation of Koçyiğit et al. (2001) that the Kura is a flexural-foreland basin loaded by the Greater Caucasus and suggests syn-Pliocene timing for the loading.

Lesser Caucasus

The Lesser Caucasus Mountains are generally interpreted as an upper Cretaceous island arc that formed during north-directed subduction along the south side of the arc (present coordinates), prior to closure of the Neotethys ocean (Robinson et al., 1995; Yılmaz et al., 2000; Golonka, 2007). The northern margin of the Lesser Caucasus is thought to be bounded by a range-front thrust fault system, but the nature of this structure is disputed. Thrusts dipping both south (Zonenshain and Le Pichon, 1986) and north (Philip et al., 1989; Jackson, 1992; Koçyiğit et al., 2001) have been proposed. The structure is also sometimes discussed in relation to the Pambak-Sevan-Sunik fault, which lies south of the range front (Fig. 1A). Geomorphic and paleoseismic studies of this fault suggest primarily dextral strike-slip motion during the Holocene (Philip et al., 2001), but the only earthquake recorded from this fault is the 1988 ($M = 6.9$) compressional event near Spitak, Armenia (Philip et al., 1992).

Reconnaissance neotectonic maps of the Lesser Caucasus and East Anatolian Plateau suggest that these regions are characterized by active E-W-striking shortening structures, such as the Lesser Caucasus range-front fault (Philip et al., 2001), NW-striking (dextral) and NE-striking (sinistral) strike-slip faults, and N-S-striking normal faults (e.g., Rebai et al., 1993; Koçyiğit et al., 2001; Copley and Jackson, 2006; Dhont and Chorowicz, 2006). It is important to note that while maps of active structures in this region agree on the general deformational style, they are inconsistent regarding the kinematics, geometry, and existence of specific major structures (e.g., Barka, 1992; Saroglu, 1992; Berberian and Yeats, 1999; Koçyiğit et al., 2001).

Greater Caucasus

A number of workers (e.g., Adamia et al., 1977; Gamkrelidze, 1986; Zonenshain and Le Pichon, 1986; Golonka, 2007) interpret the Greater Caucasus to have formed by tectonic inversion of a former backarc ocean that originally opened during north-dipping subduction of Neotethys along the southern margin of the Lesser Caucasus arc. The timing of cessation of subduction and subsequent shortening and

tectonic inversion of the Greater Caucasus basin are poorly defined, with estimates ranging from the late Eocene (Lozar and Polino, 1997; Saintot and Angelier, 2002) to the Pliocene (Philip et al., 1989), but with most estimates focusing on the Oligocene (e.g., Adamia et al., 1977; Vincent et al., 2007) or Miocene (e.g., Kopp and Shcherba, 1985; Ershov et al., 2003; Meulen-kamp and Sissingh, 2003). The spatial evolution of Greater Caucasus exhumation is also unclear, with hypotheses including: two distinct exhumation events with the western half of the range being exhumed before the eastern half (Král and Gurbanov, 1996), a single continuous exhumation event that began near the midpoint of the range and propagated laterally toward the eastern and western ends (Hovius and Allen, 2000), or a single exhumation that began in the west and gradually propagated eastward (Allen et al., 2003). Limited low-temperature, thermochronologic data seem to support the hypothesis of eastward propagation of exhumation in the Greater Caucasus, with apatite fission-track ages that progressively young from the middle to late Miocene from the western to central Greater Caucasus (Král and Gurbanov, 1996), and Pliocene (U-Th)/He ages in the eastern Greater Caucasus (Avdeev and Niemi, 2008). The low-temperature thermochronologic results are also consistent with recent provenance studies within the lower Pliocene Productive Series of Azerbaijan and the South Caspian, which suggest significant uplift and erosion of the eastern Greater Caucasus occurred as recently as the late Pliocene (Morton et al., 2003; Hinds et al., 2007).

Estimates of Total Shortening

Previous estimates of total shortening across the Caucasus are uncertain, ranging from 130 to 200 km across the Greater Caucasus to 200–900 km across the combined Lesser and Greater Caucasus. We are aware of only one geologically based total shortening estimate across the Greater Caucasus, in which Dotduyev (1986) estimated 200 ± 50 km of shortening based on palinspastic reconstructions. Sobornov (1994) used reconstructions based on seismic sections and well log data to estimate that the Dagestan thrust system (Fig. 1B), located along the northeast margin of the Greater Caucasus, has accommodated 20–50 km of shortening. Allen et al. (2004) extrapolated this percent shortening estimate across the entire Greater Caucasus to arrive at ~ 130 km of total shortening. Estimates for total shortening across the Greater and Lesser Caucasus as a whole are similarly poorly constrained. Bazhenov and Burtman (1989) originally suggested a total of 900 ± 350 km of

shortening across the Lesser and Greater Caucasus, based on paleomagnetic data from the Lesser Caucasus. Improvements in technique allowed Bazhenov and Burtman (2002) to refine this estimate to ~ 400 km of total shortening, based on a synthesis of Dotduyev's (1986) shortening estimates and paleomagnetic evidence of oroclinal bending of the Pontide-Lesser Caucasus arc, which was first described by Adamia et al. (1979) and Asanidze and Pecherskiy (1979). Finally, Ershov et al. (2003) used area balancing of crustal scale sections from seismic lines to estimate between 200 and 300 km of total shortening across the Lesser and Greater Caucasus.

Present-Day Velocity Field

Previous work has focused on using patterns of seismicity and/or geodetic measurements to determine the present-day kinematics of deformation within the central sector of the Arabia-Eurasia collision zone (e.g., McKenzie, 1972; Westaway, 1990; Jackson, 1992; Priestley et al., 1994; Westaway, 1994; Jackson and Ambraseys, 1997; Jackson et al., 2002). Convergence rates determined from seismicity are significantly smaller than those estimated by geodetic methods. For example, Westaway (1990) used magnitudes of historic and recent earthquakes paired with reconnaissance field observations in Armenia to suggest that the Caucasus are shortening at 2–3 mm/a, with a maximum possible rate of 6 mm/a. Westaway (1990) further proposed that only 1 mm/a of this shortening was concentrated in the Kura Basin in Azerbaijan. In contrast, more recent GPS measurements imply significantly faster shortening rates. Studies by McClusky et al. (2000), Reilinger and Barka, (1997), and Reilinger et al. (1997, 2004) report a total of ~ 10 mm/a of NE-SW shortening, with ~ 6 mm/a in the Greater Caucasus and ~ 4 mm/a in the Lesser Caucasus. Likewise, Vernant et al. (2004) report 14 ± 2 mm/a of N-S convergence across the eastern Greater Caucasus. The most recent GPS-derived velocity fields in the Caucasus region indicate that the rate of convergence between the Lesser and Greater Caucasus increases eastward, from ~ 4 mm/a in the Rioni basin, Georgia, to ~ 14 mm/a in the Kura Basin, Azerbaijan (Fig. 2, Reilinger et al., 2006). These data further suggest that both the Greater and Lesser Caucasus are subject to minimal internal deformation (Fig. 2, Reilinger et al., 2006), implying major shortening structures lie between the two ranges. Reilinger et al. (2006) fit an elastic block model to the velocity field and concluded that the Lesser Caucasus and part of the East Anatolian Plateau behave rigidly and rotate counterclockwise at $0.84^\circ/\text{Ma}$ relative to stable Eurasia about an Euler pole in

the eastern Black Sea (42.1°N , 37.8°E , Fig. 2). The northern boundary of this block is located along the southern front of the Greater Caucasus range and illustrated as a north-dipping thrust (Fig. 2, Reilinger et al., 2006). Allmendinger et al. (2007) used the same velocity field to calculate 2-D dilational strain and vertical-axis rotation fields. This analysis also identified the Lesser Caucasus and East Anatolian Plateau as areas of counterclockwise rotation, with similar NE-SW shortening rates as suggested by the block model ($\sim 0.8^\circ/\text{Ma}$). Calculated strain rates are low throughout the eastern Caucasus, reaching their maximum along the southeastern range front of the Greater Caucasus and within the Kura fold-thrust belt. Within the Kura Basin and southeastern Greater Caucasus, strain rates increase eastward, mirroring the eastward increase in velocity.

Current GPS station coverage is too sparse to resolve the major compression structures accommodating shortening between the Greater and Lesser Caucasus. It is generally presumed that most of this shortening occurs on faults along the southern range front of the Greater Caucasus (Jackson, 1992). Alternatively, deformation may be localized within the Kura fold-thrust belt, a conspicuous belt of topography that has previously been described but discounted as the locus of significant shortening (e.g., Dotduyev, 1986; Westaway, 1990). To evaluate the importance of the Kura fold-thrust belt in absorbing Arabia-Eurasia convergence, we used remotely sensed data and virtual-terrain software to study this region.

NEOTECTONICS OF THE KURA FOLD-THRUST BELT

Methods

To make numerous observations of detailed (50–500 m) geomorphic features over a large portion (75 km by 300 km) of the thrust belt, we used the Real Time Interactive Mapping System (RIMS) software (Bernardin et al., 2006) to produce a neotectonic map of the Kura fold-thrust belt (Plate 1¹). No new fieldwork was conducted. RIMS provides a virtual terrain model that is created by draping a texture image (e.g., a satellite image or air photo mosaic) over a digital elevation model (DEM) in a format similar to the one used in Google Earth (<http://earth.google.com/>). RIMS allows users to manipulate (e.g., rotate, pan, zoom) and dynamically adjust vertical exaggeration of the virtual terrain model at the full resolution of the data in real time (i.e., without

¹Plates 1 and 2 are on a separate sheet accompanying this issue.

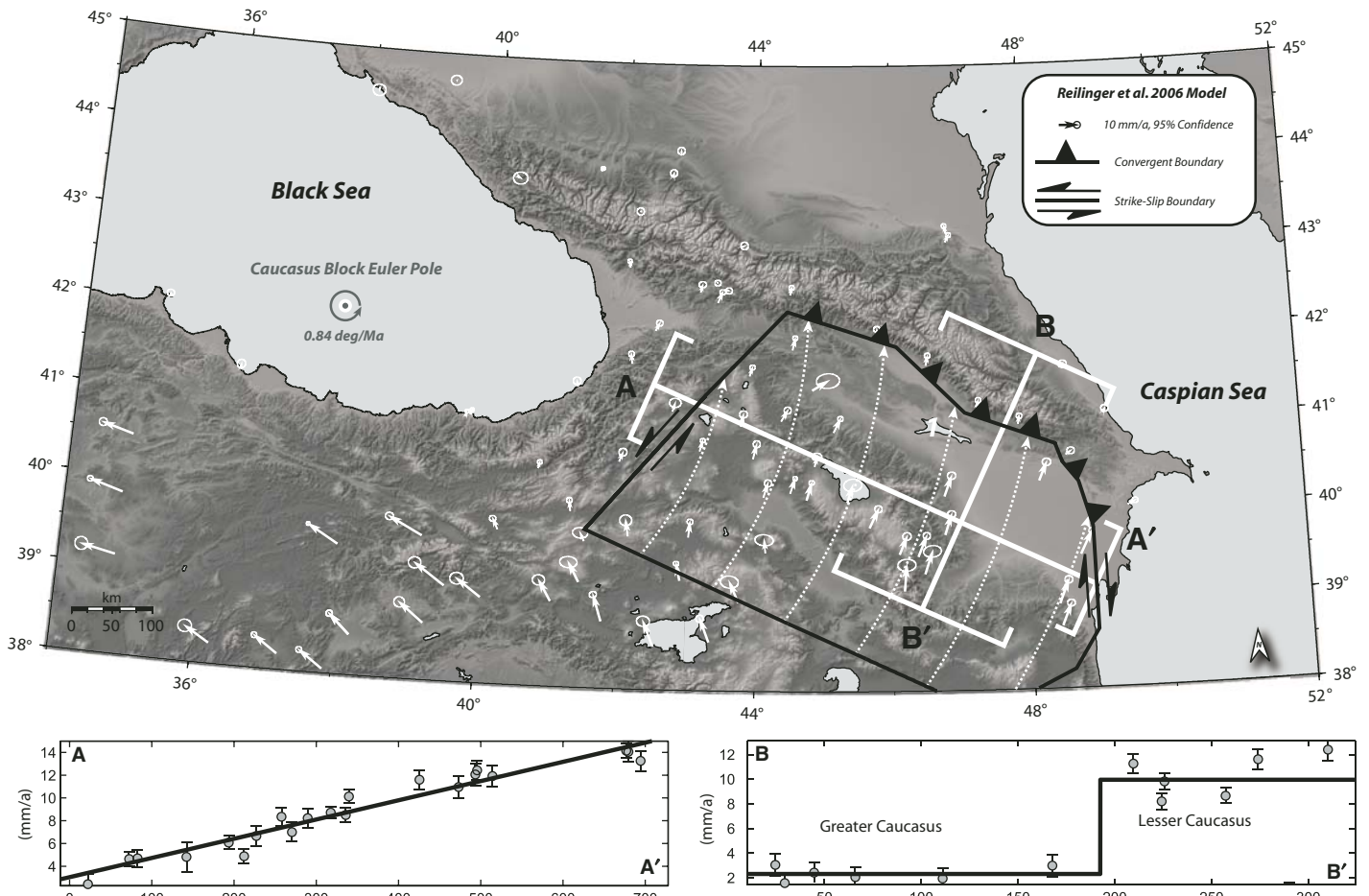


Figure 2. Map showing global positioning system (GPS) velocities (white arrows) relative to Eurasia and rigid block model (black polygon) reported by Reilinger et al. (2006). Dashed white lines are contours of equal velocity about local pole of rotation. White lines show profiles along (A–A′) and across (B–B′) strike of the Caucasus, with brackets on ends of profile lines delineating boundaries of box, within which data were collapsed onto the profile line. Plots show velocity components along each profile with 1-sigma errors. Profile A–A′ indicates an eastward increase in shortening rates along the southern margin of the Greater Caucasus mountains. Profile B–B′ indicates that at the position of the profile, the Lesser Caucasus move northward ~7 mm/a faster than the Greater Caucasus, suggesting a zone of active shortening between the two ranges. Reilinger et al. (2006) used this observation, coupled with the relatively homogeneous velocities across the Lesser Caucasus, to propose that the Lesser Caucasus and portion of the East Anatolian Plateau are rotating counterclockwise as a semirigid block at a rate of 0.84°/Ma about an Euler pole in the Black Sea. Kinematics of the block boundaries are generalized from the fault normal and parallel slip rates implied by the block model and reported by Reilinger et al. (2006). Velocity field, profiles, and block boundaries modified from Reilinger et al. (2006). Base hillshade image generated from Shuttle Radar Topographic Mission (SRTM) 90-m digital elevation model (DEM).

needing to wait for the view to refresh). RIMS also provides several mapping tools that facilitate analysis of digital terrain data. For example, users can record observations by drawing georeferenced and attributed polylines directly on the digital terrain model, while simultaneously interacting with data via the terrain visualization system. In addition, RIMS also provides a “virtual geologic compass” (VGC) tool for measuring the orientations of surfaces or beds by interactively fitting a measurement plane to a topographic surface or the line of intersection between a dipping bed and the topography

(Fig. 3B). For a complete description of RIMS, see Bernardin et al. (2006) and the RIMS software distribution site at <http://keckcaves.org/software/RIMSG3/>.

We built virtual terrain models from two different data sets, analyzed them in RIMS, compiled the resulting maps in a geographic information system (GIS), and post-processed the mapping using standard drafting software to create the neotectonic map shown in Plate 1. The first RIMS project paired three arcsecond (~90 m/pixel) DEM data from the Shuttle Radar Topographic Mission (SRTM) (Farr

et al., 2007) with a false-color hillshade image produced from the same data. The SRTM data were obtained from Consultative Group on International Agricultural Research (CGIAR) (Jarvis et al., 2006), available from <http://srtm.csi.cgiar.org>. The second project paired 15 m/pixel ASTER VNIR data with 30 m/pixel ASTER DEM (Yamaguchi et al., 1998; Hirano et al., 2003). We used L1B ASTER data obtained from National Aeronautics and Space Administration’s (NASA) Warehouse Inventory Search Tool (see <https://wist.echo.nasa.gov/~wist/api/imswelcome/>).

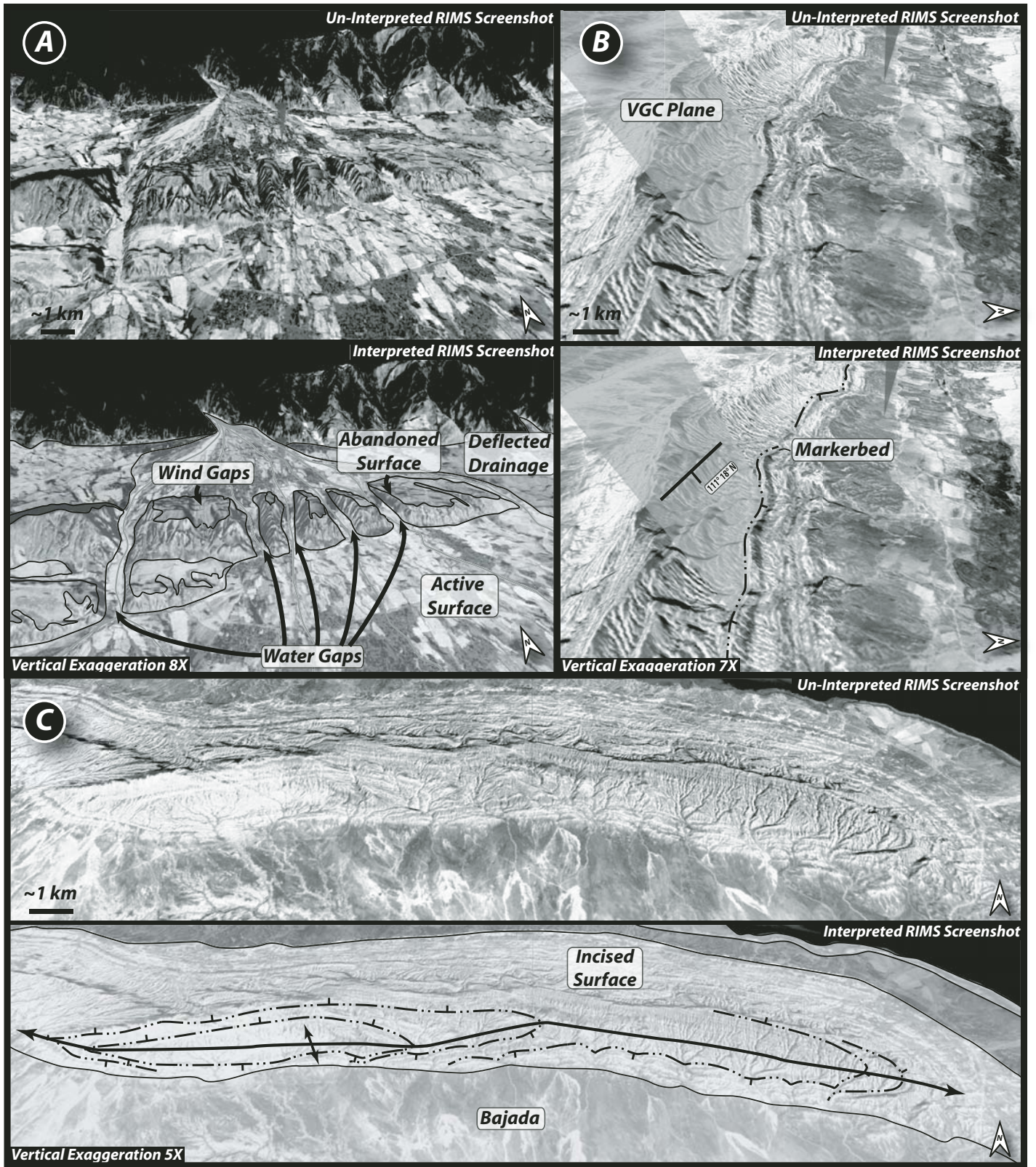


Figure 3. Uninterpreted (top) and interpreted (bottom) screenshots from the Real-Time Interactive Mapping System (RIMS), taken at vantage points shown in Plate 1. Vertical exaggeration of terrain display is indicated in lower-left corner. Digital terrain models generated from false-color (R—Band 3N, G—Band 2, B—Band 1) Advanced Spaceborne Thermal Emission and Reflection Radiometer (ASTER) visible to near-infrared (VNIR) imagery draped over ASTER digital elevation model (DEM). Refer to Plate 1 for a description of the colors used in the interpreted images in the color version of this figure. Note that due to perspective, scale bars are approximate. (A) View looking north at a set of water and wind gaps located where the Girdiman River crosses an actively growing fold at the east end of the Kura fold-thrust belt. Preserved surfaces along the fold crest are examples of abandoned surfaces. Alluvial fans both north and south of the fold are examples of active surfaces. Note drainage deflection around eastern tip of fold. (B) View looking west along the northern limb of an anticline exposed on the west bank of the Mingachevir Reservoir. Transparent plane shows the Virtual Geologic Compass (VGC) tool available in Real-Time Interactive Mapping System (RIMS). In this case, the VGC plane is fit to the trace of a dipping marker bed where it crosses two north-flowing gullies. (C) View to north of the same anticline as in Part B with broad bajada complex exposed at the southern range front. By tracing and measuring exposed marker beds, the axial trace of this doubly plunging anticline can be mapped from the digital terrain data using RIMS. A color version of this figure is available in the GSA Data Repository.



Our mapping strategy focused on finding and then documenting deformed landforms using the RIMS visualization environment. Specific goals were to (1) establish structural geometries and styles, (2) evaluate the extent to which tectonic landforms indicate the structures are active, and (3) investigate the relative ages of structures along strike. To identify structures and define their geometries, we mapped continuous marker beds visible in the ASTER imagery (Fig. 3C) and then measured bedding orientations in RIMS by fitting the VGC tool to bedding traces at locations where the markers cross rugged topography (Fig. 3B). We also mapped drainage deflections and water and wind gaps to help evaluate the activity and relative ages of structures (Fig. 3A, Burbank et al., 1996; Jackson et al., 1996).

In the case of unconsolidated Quaternary deposits, the degree of incision or roughness of a

geomorphic surface (e.g., on alluvial fans or fluvial terraces) can serve as a proxy for the relative surface age (Burbank et al., 1999; Keller et al., 1999; Frankel and Dolan, 2007), with more incised and thus rougher surfaces generally being older relative to those constructed more recently. Thus, to further constrain structural activity and investigate along-strike variability in relative ages and/or rates of deformation within the study area, we developed a scheme for classifying topographic surfaces, and then mapped the distribution of these units in RIMS. The scheme is based on the long-wavelength planarity of the surface (i.e., one that is planar at the tens of kilometers scale) and its degree of incision, elevation relative to local drainages, and the extent to which bedding traces were discernable. Our assumption is that the degree of incision, surface elevation, and bedding exposure all increase

with increasing age for a preserved geomorphic surface. We distinguished four different types of geomorphic surfaces, examples of which are shown in Figure 4. (1) *Active* surfaces are planar, show minimal to no incision, and grade to the local channel network. (2) *Abandoned* surfaces are also planar at long wavelengths but are elevated above, and locally incised by, the active channel network. When folded, abandoned surfaces can slope more steeply than active ones. (3) *Queried* and abandoned surfaces are similar, in that both are smooth at long wavelengths but differ in that their structural or geomorphic context renders a Quaternary age unlikely for queried surfaces, such as on dip slopes supported by resistant beds within an exposed fold. (4) *Incised* surfaces have high local relief and thus span areas dissected by the active drainage network. Incised areas with bedrock hillslopes typically expose marker beds that can be used to delineate the underlying structural geometry. We interpret abandoned surfaces as being relatively older than active ones, with both being of probable Quaternary age. In contrast, we apply no relative or absolute age interpretation to the queried and incised surfaces.

By combining marker bed geometries with the spatial distribution of the geomorphic surfaces, we identified the axial traces of folds and estimated the relative activity of the underlying structures. We identified syncline and anticline axial traces based on marker bed dips measured with the VGC tool (Fig. 3C). We mapped traces of the axial surfaces of folds using both observations of reversals in bedding dip direction and points of maximum curvature along marker beds in fold closures. If a fold nose was traceable using marker beds, we also recorded the plunge direction of the fold (Fig. 3C). Structures that we interpreted as folds but that lacked clear evidence of dip reversal were mapped as inferred (Plate 1). The distinction between active (red)

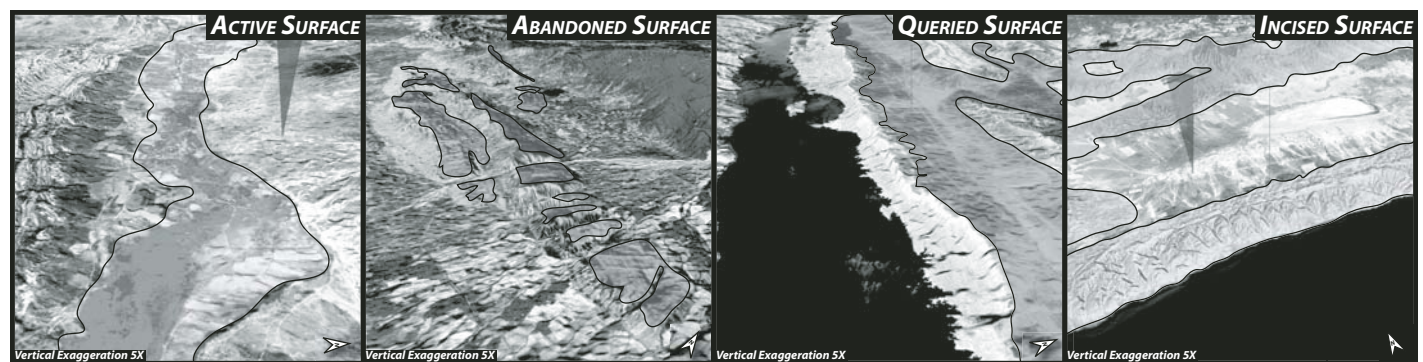


Figure 4. Screenshots from Real-Time Interactive Mapping System (RIMS) showing examples of the different types of mapped surfaces. See text for explanation of surfaces. Same digital terrain data as in Figure 3. Note that the gray triangles are artifacts from RIMS and do not denote any particular features of interest. A color version of this figure is available in the GSA Data Repository.

and inactive (black) fold axes on Plate 1 is based on whether or not the fold deforms abandoned surfaces, the rationale being that deformation of abandoned surfaces implies that the most recent increment of fold growth occurred in the Quaternary. Folds that do not deform abandoned surfaces were mapped as inactive, although this is an admittedly imprecise method of determining fold activity because the absence of abandoned surfaces mantling a fold could also result from rates of erosion that outpace fold growth. However, this conservative approach minimizes the risk of overestimating fold activity within the belt. Likewise, we did not map fault traces in RIMS because the data were of insufficient spatial resolution to permit identification of fault scarps and because we were concerned that linear slope-breaks along the forelimbs of folds may reflect axial traces of active synclines, rather than faults.

Results of Neotectonic Mapping

Our neotectonic mapping documents that the Kura fold-thrust belt comprises a series of range-parallel (WNW-ESE-trending), south-verging folds, as suggested by previous authors (e.g., Dotduyev, 1986; Philip et al., 1989; Tevelev and Blyumkin, 1990; Ershov et al., 2003). Our mapping further indicates that the neotectonic geology of the Kura fold-thrust belt varies along strike.

The folds occur as either anticline-syncline pairs or isolated anticlines (Plate 1). Exposed axial traces of folds extend along strike for 20–50 km, with fold widths of 5–10 km. Although the folds are open, with shallowly dipping limbs (10° – 20°), anticlines typically verge to the south, as indicated by southern limbs that dip 5° – 10° more steeply than limbs to the north. Most folds in the area plunge, and some are doubly plunging, but there is no clear regional trend in plunge direction. In contrast, there is a trend in the number of exposed folds, which decrease eastward from 11 in the west along section A–A' to three in the east along section B–B' (Plate 1).

The geomorphic expression of folds also changes systematically from west to east. In the west, most folds are expressed in bedrock or heavily incised surfaces (Plate 1). Anticlines in this region commonly coincide with topographic ridges with crests located near the core of the anticline. These ridges are typically asymmetric across strike, with gently dipping topographic slopes on the northern limbs (1° – 10°) and steeper slopes on the southern limbs (15° – 25°). Bedding in the southern limbs is almost completely obscured by coalesced alluvial fan complexes (bajadas) at the base of the ridges

(Fig. 3C). In the east, folds are topographically expressed as slightly asymmetric, smooth ridges that are almost completely mantled by queried or deformed abandoned surfaces and that expose minimal bedrock (Figs. 3A and 4). Folds in the west are more incised than those in the east and generally lack a deformed mantle of inferred Quaternary sediments (Plate 1).

In addition, both drainage patterns and the number of wind and water gaps change systematically along strike (Plate 1). In the west, the drainage pattern is dominated by the Alazani, Kura, and Iori rivers, which are SE-flowing, longitudinal drainages (i.e., streams that flow parallel to fold axes). The Iori and Kura rivers do not cross any mapped shortening structures, but the Alazani River makes an $\sim 90^{\circ}$ turn to flow south into the Mingachevir Reservoir. West of this southward bend, no transverse drainages (i.e., streams that flow perpendicular to fold axes) cross the entire Kura fold-thrust belt. In contrast, east of this bend, five transverse drainages with headwaters in the Greater Caucasus cross the fold-thrust belt. Between the Alican and Turyan rivers, a number of wind gaps are preserved on the crests of folds along the northern margin of the Kura fold-thrust belt (Plate 1 and Fig. 5). North of these wind gaps and within the Alazani Basin, tributaries of the transverse rivers are typically deflected where they intersect the north limbs of the folds (Fig. 5).

The cross-strike topographic width of the Kura fold-thrust belt also systematically decreases eastward, from 65 km in the west to 25 km in the east (Plate 1). In addition, the volume of topography above the Kura and Alazani basins also decreases eastward, as demonstrated by the strike-perpendicular topographic profiles shown in Plate 1. These profiles show the area bounded above by the present topographic surface and below by a southward-sloping line extrapolated from the floors of the Alazani and Kura basins, which flank the topographically expressed fold-thrust belt. The floors were defined as the mean topographic surface outside the confines of the fold-thrust belt. These topographic areas differ by a factor of 3 along strike, from ~ 14 km² in the west to ~ 4 km² in the east (Plate 1).

We also attempted to assess the activity of the Greater Caucasus range-front fault system by measuring mountain-front sinuosity (Bull and McFadden, 1977) along the southern slope of the eastern Greater Caucasus (Fig. 6). Using a methodology modified from Wells et al. (1988), we divided the range front into six equal-length (50-km-long) segments in order to assess along-strike variability in sinuosity. There is a systematic eastward decrease in sinuosity along the southern range front of the Greater Caucasus, decreasing from 3.2 to 1.9, with a significantly

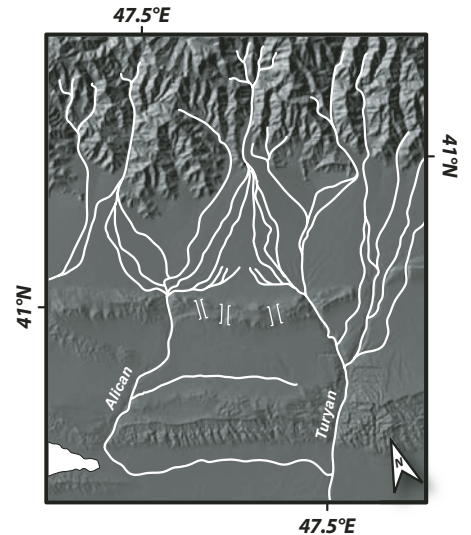


Figure 5. Map of Kura fold-thrust belt between the Alican and Turyan rivers. White brackets indicate locations of wind gaps along crest of northern anticline. Note the fan-shaped drainage networks on the north side of this anticlinal ridge, formed by drainage defeat and deflection during active fold growth. Hillshade image generated from Shuttle Radar Topographic Mission (SRTM) 90-m digital elevation model (DEM) with drainages highlighted in white.

less sinuous range front (1.1) measured to the east of the termination of the Kura fold-thrust belt (Fig. 6).

Interpretation of Neotectonic Activity

Two main conclusions can be drawn from our neotectonic mapping. First, the Kura fold-thrust belt records active deformation along the southern flank of Greater Caucasus. The sinuosity of the Greater Caucasus mountain front and the absence of clearly deformed fans along this margin suggest that the active thrust front has propagated south, away from the Greater Caucasus range front. Second, neotectonic proxies for total shortening within the belt systematically decrease eastward within the belt, an interpretation that is further supported by geological observations presented in “Bedrock Geology of the Kura fold-thrust belt,” below.

The results of the mountain-front sinuosity assessments along the southern range front of the Greater Caucasus suggest that active deformation has progressively moved southward from the Greater Caucasus range front to the Kura fold-thrust belt (Fig. 6). Slip on an active range-front fault will tend to produce a relatively undissected mountain front, corresponding to a

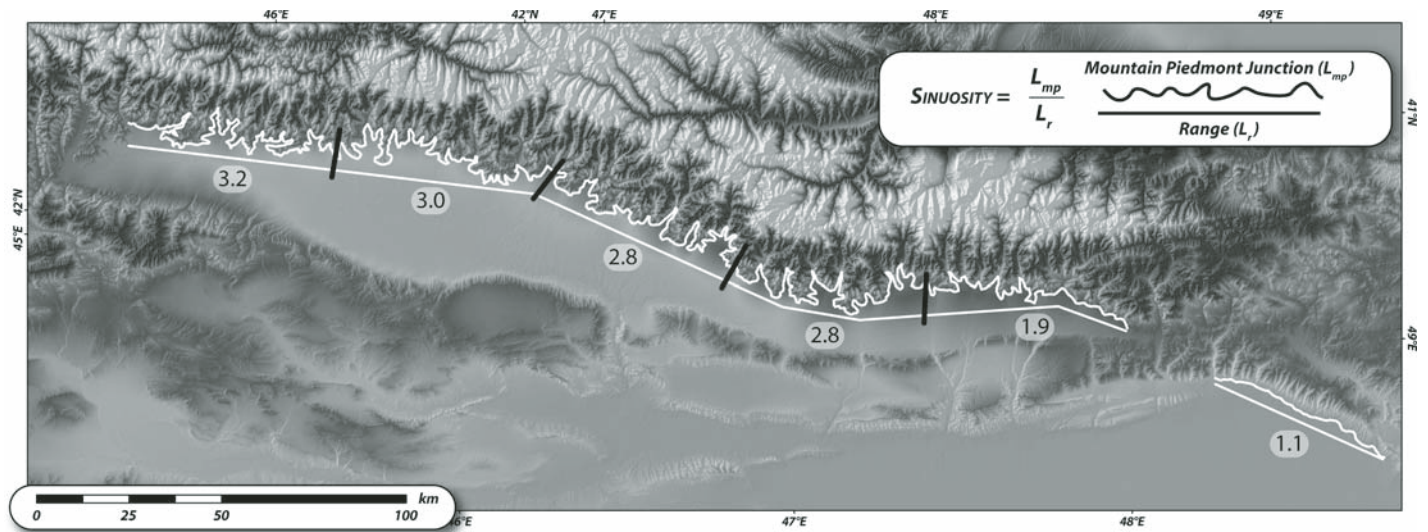


Figure 6. Mountain-front sinuosity of the southern range front of the Greater Caucasus. Each “range” segment is 50 km long. There is a progressive eastward decrease in sinuosity along the Greater Caucasus range front directly north of the Kura fold-thrust belt, which suggests that there is a corresponding eastward increase in the relative activity of the Greater Caucasus range-front fault system. The sinuosity of the range front to the east of the Kura fold-thrust belt is very close to one, indicating that this section of the range-front fault system is relatively active. Equation for sinuosity from Burbank and Anderson (2001).

sinuosity near one, whereas a less active fault will be characterized by a more embayed mountain front, with a sinuosity greater than one (Bull and McFadden, 1977). The measured sinuosity suggests that (1) the section of the Greater Caucasus range-front fault system that lies directly to the north of the Kura fold-thrust belt is less active than associated range-front faults to the east of the termination of the Kura fold-thrust belt, and (2) the eastward decrease in sinuosity may suggest that over time there has been an eastward-propagating transfer of slip from the Greater Caucasus range front to the Kura fold-thrust belt.

Our conclusion that structures within the Kura fold-thrust belt are active is supported by folded abandoned surfaces of probable Quaternary age, drainage patterns, and ephemeral geomorphic features such as wind gaps. Actively growing folds can both perturb drainage networks and produce distinct geomorphic markers such as water and wind gaps (Fig. 3A) attesting to fold activity (e.g., Burbank et al., 1996, 1999; Jackson et al., 1996; Keller et al., 1999). Because wind gaps will be subject to erosion once formed, they are ephemeral features within tectonically active landscapes. Thus, the wind gaps we have identified and mapped in Plate 1 attest to recent deformation within the Kura fold-thrust belt. Another diagnostic feature of drainage networks affected by active folds is the development of a distinctively lopsided catchment shape over time as large drainages progressively capture defeated drainages

(Fig. 5, Jackson et al., 1996; Keller et al., 1999). Thus, the drainage patterns shown in Figure 5 are also consistent with our conclusion that the Kura fold-thrust belt is active. The catchment pattern of the Alazani River in the western portion of the Kura fold-thrust belt is asymmetric in this way (i.e., most of the drainage area is to the north, within the Greater Caucasus), and this gross consistency with this model of evolving drainage networks in regions of active folding further supports our conclusion of active deformation within the Kura fold-thrust belt.

Our interpretation of along-strike variation in total shortening is supported by the systematic along-strike variations in the neotectonic geology, geomorphology, and topography of the Kura fold-thrust belt. The larger number of structures, cross-strike width, and topographic volume above base-level of the western portion of the belt relative to the eastern sector are all most simply explained by higher magnitudes of total shortening in the west than the east. One alternative interpretation is that these along-strike variations stem from changes in structural style, with thin-skinned thrusting in the west versus thick-skinned deformation in the east. However, our mapping does not support this idea because the wavelengths (average 10 km distance from anticline axis to anticline axis) and axial-trace lengths (~20–30 km) of the folds are generally similar along strike (Plate 1).

Another possible alternative interpretation is that the along-strike variations stem from

changes in erosion rate. For example, the greater degree of incision and absence of wind gaps in the western part of the belt might reflect higher erosion rates in this area relative to the east. However, we see three problems with this idea. First, patterns of historical precipitation appear to be broadly uniform along strike (Borisov, 1965; Lydolph, 1977). Borisov (1965) reported similar mean annual precipitation (~400 mm/a) throughout the Kura Basin region, with precipitation spread out over a longer time period near the Caspian coast than more inland, where precipitation occurs during a shorter rainy season. The boundary between these two zones is roughly 48°E (Borisov, 1965), although Lydolph (1977) places it farther east. Thus, most, if not all, of the Kura fold-thrust belt lies within the rainy-season zone. Second, rocks should be less prone to erosion in the west than the east. As we show below in “Bedrock Geology of the Kura fold-thrust belt,” there is a westward increase in stratigraphic depth of exposure within the thrust belt. These more deeply buried rocks are likely to be more indurated than younger and shallower rocks exposed in the eastern part of the belt. Third, along-strike variation in erosion fails to explain all of the along-strike variation in the belt. Critical-taper wedge models of orogenic belts (Davis et al., 1983; Dahlen, 1990) show that increased erosion rates tend to localize deformation, narrow the cross-strike width of the thrust belt, and reduce topographic volume, if all other variables are held fixed (Dahlen

and Suppe, 1988; Beaumont et al., 1991). Thus, the higher erosion rates in the west needed to explain the greater degree of incision and absence of wind gaps seem incompatible with the larger number of shortening structures, greater width, and higher topographic volume of the fold-thrust belt in this area.

Although we argue that the simplest explanation for the along-strike variation in the neotectonic structures, geomorphology, and topography of the Kura fold-thrust belt is a corresponding eastward decrease in total shortening, our observations alone fail to resolve the relative importance of rate versus initiation age in producing the variable total shortening. For example, the eastward decrease in the number of shortening structures could have been produced by either faster rates or earlier onset of shortening in the west relative to the east. Likewise, the eastward decrease in the degree of incision and the increase in the number of wind gaps could either indicate that deformation is faster in the west than the east (presuming that faster shortening rates will generally lead to steeper slopes and thus higher degrees of incision), or that deformation youngs eastward. Variations in drainage network morphology are similarly ambiguous, because either variable rate or initiation age can explain the eastward transition from longitudinal to transverse drainage patterns. Faster rates of shortening should lead to greater degrees of stream defeat and thus more developed longitudinal drainages, all other variables being equal. Alternatively, along-strike variation in the timing of deformation may produce systematic variations in the depth of exposure and thus resistance to erosion that can lead to the development of longitudinal drainages as older parts of the belt are progressively exhumed (e.g., Oberlander, 1985). Finally, variations in the cross-strike width and volume of the fold-thrust belt can also be explained by either variable rate or timing because both can lead to along-strike variation in total shortening.

In summary, our neotectonic mapping indicates that the Kura fold-thrust belt comprises a sequence of range-parallel, south-verging folds that defines the active deformation front along the south flank of the Greater Caucasus. Along-strike variations in the neotectonic structures, geomorphology, and topography of the belt are most simply explained by systematically eastward-decreasing total shortening. However, the relative importance of along-strike variations in the rate and/or timing of shortening in producing this variation in total shortening remain unclear. To test these interpretations and further constrain the late Cenozoic structural evolution of the Kura fold-thrust belt, we paired our neotectonic observations with published information regarding the

regional stratigraphy and geology to construct two balanced cross sections across the Kura fold-thrust belt. Specific goals were to (1) develop preliminary quantitative estimates of total shortening within the belt to test the interpretation that total shortening decreases eastward along strike, (2) determine the relative importance of along-strike variation in the rate and/or timing of deformation within the belt, (3) explore potential along-strike variations in structural style, and (4) evaluate the extent to which significant shortening structures may be buried at the eastern end of the belt, and thereby test our conclusion that variation in the number of exposed structures and cross-strike topographic width of the belt reflects variable total shortening.

BEDROCK GEOLOGY OF THE KURA FOLD-THRUST BELT

Stratigraphic Framework

The first step in constructing the balanced cross sections was to establish the regional stratigraphic framework. We followed previous work in using names for the sedimentary units that are the same as those for the regional stage divisions (e.g., Nalivkin, 1973; Agabekov et al., 1976; Jones and Simmons, 1996; see Fig. 7). These stages are defined primarily on the basis of the biostratigraphy of Paratethys (Jones and Simmons, 1996). Units of particular importance to the current study include the Kimmerian (i.e., Productive Series of Azerbaijan), the Akchagyl (or Akchagyl), and the Apsheronian (or Apsheron or Absheron in some literature).

It is important to note that there are significant uncertainties in correlations between these regional stages and absolute ages. There also exists the potential for diachroneity within the regional stages of the Paratethys. For example,

in the Paratethyan stratigraphy preserved in the Carpathian foredeep basin in Romania, Vasiliev et al. (2004) used high-resolution magnetostratigraphy to illustrate that the duration of the Pontian stage in this location was significantly shorter than suggested by the review of Paratethyan stratigraphy presented by Jones and Simmons (1996). These authors also showed that, in general, the absolute age boundaries and duration of regional stages within Paratethyan stratigraphy may vary substantially between locations. Within the central Arabia-Eurasia collision, Mitchell and Westaway (1999) suggest that the transition between Kimmerian and Akchagyl sediments occurred at 2 Ma (as opposed to 3.4 Ma as reported by Jones and Simmons, 1996) and that the transition from Akchagyl to Apsheron occurred at 1.2 Ma (as opposed to 1.6 Ma), based on K/Ar dating of Pleistocene volcanics in the Lesser Caucasus mountains of Armenia and their possible correlation to volcanic units elsewhere in the Caucasus. The robustness of this proposed revision remains unclear, and given the potential for wide variation in the absolute age of stage boundaries, we have chosen to use the correlations presented by Jones and Simmons (1996) because they represent a homogeneous average estimation of the stage durations and boundaries. Because the correlation between regional stages and absolute ages and global epochs are questionable and continually evolving, we choose to generally speak in terms of regional stages but use these correlations when deriving rates of deformation.

Limited descriptions are available in the international literature of individual formations within either the Kura or South Caspian basins. Our compilation of regional stratigraphic data is based primarily on syntheses reported by Agabekov et al. (1971, 1976), Azizbekov (1972), Agabekov and Moshashvili (1978),




Figure 7. Compilation of published stratigraphic information for the Kura Basin. First column indicates global chronostratigraphic epochs from the 2004 International Commission on Stratigraphy time scale (Gradstein et al., 2004). Second column provides names of regional stages and ages of stage boundaries for the South Caspian and Kura basins from Jones and Simmons (1996). Third column lists unit abbreviations, modified from Nalivkin (1976). Columns four through six provide three different estimates for unit thicknesses within the Kura Basin. Values in the fourth column are from a summary by Azizbekov (1972) of thicknesses measured in well logs and exposures throughout the Kura Basin; those in the fifth column are compiled from thicknesses measured in the Saatly and related wells (Fig. DR1 [see footnote 1]) (Agabekov and Moshashvili, 1978); and those in the sixth column are from that portion of the Kura Basin that lies east of the West Caspian Fault (Fig. 1B) and extends into the South Caspian depression (Inan et al., 1997). Columns seven and eight list unit thicknesses used to construct the balanced cross sections, and were compiled from the values in columns four to six, isopach maps (Agabekov et al., 1976), and interpretation of the Nalivkin (1976) geologic map coupled with dip data from our neotectonic mapping. Column nine lists key observations about the stratigraphic units that were important in the construction of the balanced cross sections.

Late Cenozoic deformation of the Kura fold-thrust belt

	REGIONAL STAGES	UNITS	KURA BASIN <small>(Azizbekov et al., 1972)</small>	SAATLY WELLS, KURA BASIN <small>(Agabekov and Moshashvili, 1978)</small>	LOWER KURA DEPRESSION <small>(Inan et al., 1997)</small>	ESTIMATED THICKNESS IN CROSS SECTION A	ESTIMATED THICKNESS IN CROSS SECTION B	KEY OBSERVATIONS	
0 Ma	PLEISTOCENE	KHVALYNAN <small>GRASS</small>	120–930 m	360–900 m	600 m	Variable	Variable	Undifferentiated colluvium (Quaternary).	
		KHAZARIAN							
		0.7 Ma							
	APHERONIAN	Qap	0–1430 m	1400–1700 m	600–1500 m	Variable	140–1400 m	Crosscuts exposures of folded strata throughout the fold-thrust belt with highly variable local thickness variations.	
	LATE PLEISTOCENE	Akchagylian	Tak	220–940 m	180–230 m	60 m	280 m	570 m	Varies in thickness and cross cuts folded strata in western extent of belt, grades into more conformable contact relations to the east. Both Apheron and Akchagyl age sediments generally increase in thickness eastwards (towards the S. Caspian basin).
	EARLY PLEISTOCENE	Kimmerian	Tk	0–4000 m	270–480 m	3000–4800 m	0 m	0 m	The Productive Series of Azerbaijan. Nalivkin (1976) does not formally map any Productive Series in the Kura fold-thrust belt. N ₂ ² , described as "Mid-Pliocene sediments," are mapped in the eastern section of the fold-thrust belt which we have correlated with Kimmerian stage.
5 Ma	LATE MIOCENE	Pontian	Tp	150–600 m	40–260 m	200 m	710 m	420 m	Within the Kura fold-thrust belt, the combination Maeotian-Pontian unit (N ₁ m + N ₂ p) is mapped, but farther east where the fold-thrust belt merges with the main range, only Pontian age sediments are mapped. Outcrop patterns and subsurface data both suggest that the Maeotian and Pontian age sediments thicken significantly to the west.
		Maeotian	Tmpo	25–500 m					
	LATE MIOCENE	Sarmatian	Ts	100–2900 m	50–80 m	0 m	1000 m	280 m	Sarmatian age sediments thicken significantly to the west, similar to the overlying Maeotian and Pontian sediments.
10 Ma	MIDDLE MIOCENE	Konkian	Tkk	25–200 m	0–415 m	1000 m	420 m	Not estimated	The vast majority of mid-Miocene units are simply mapped as N ₂ ² which encompasses the four regional stages (Konkian, Karaganian, Chokrakian, Tarkhanian). Within the Kura fold-thrust belt, exposures of mid-Miocene units are generally thin, probably not exceeding 500 meters in total thickness. The mid-Miocene units reach their maximum thickness (1000 m) farther south within the Kura Basin. Based on mapped exposure and estimations of depth-to-detachment, the base of the mid-Miocene strata is hypothesized to be the detachment horizon in the western cross section.
		Karaganian	Tkkct	50–350 m					
		Chokrakian	Tct	25–500 m					
		Tarkhanian		5–60 m					
15 Ma	EARLY MIOCENE	Maykopian	Tmk	1470–3200 m	0–715 m	1000–1500 m	Not estimated	Not estimated	Maykopian age sediments are the likely source rock for the Productive Series (Jones and Simmons, 1996). Devlin et al. (1999) suggested that the Maykop serves as the detachment horizon in the South Caspian basin, but the lack of mapped exposure of Maykopian sediments throughout most of the Kura fold-thrust belt suggests that the detachment horizon is stratigraphically above the Maykop in the Kura basin.

Jones and Simmons (1996), Inan et al. (1997), and Gasanov and Alyyeva (2003). Descriptions of the data used from each of these references can be found in the GSA Data Repository².

Along the cross-section lines we have augmented the compiled stratigraphic information by calculating unit thicknesses using bedding orientations determined with the VGC tool in RIMS and outcrop widths as measured from the geologic map of Nalivkin (1976). Unit thicknesses calculated in this way fell within the range of previously reported values (Fig. 7).

Within the Kura fold-thrust belt, pre-Akchagyl deposits do not appear to exhibit abrupt lateral variations in thicknesses (e.g., Fig. DR1 [see footnote 1]). In contrast, abrupt lateral thickness variations are evident within the overlying Akchagyl and Apsheron units. Isopach maps (Agabekov et al., 1971) suggest that Akchagyl sediments locally vary in thickness by up to 100 m across structures at the western end of the belt but appear to have conformable contacts and relatively constant thickness to the east. By contrast, at both ends of the belt, overlying Apsheronian and Quaternary sediments locally vary in thickness by up to ~1000 m across individual structures.

Geologic and Structural Framework

As with the stratigraphic information, detailed geologic maps of the Kura fold-thrust belt are not widely available. Although a 1:200,000-scale series of geologic maps has been published by the Russian Geological Research Institute, the series does not cover key portions of the Kura fold-thrust belt, and the maps that are available predate 1960. To our knowledge, the most comprehensive and regionally extensive geologic map is that compiled by Nalivkin (1976) and published at 1:500,000 scale. Although this map shows the spatial distribution of units in some detail (i.e., at stage level), it contains minimal structural information. In particular, it lacks axial traces of folds, bedding orientations, and information regarding the type and style of faulting. Complete topographic data are also absent, although major drainages are shown.

Plate 2 (see footnote 1) shows a new geologic map of the Kura fold-thrust belt, which we compiled by merging the structural geometries determined using RIMS with the contact locations and unit assignments from the Nalivkin map (Data Repository [see footnote 1] provides a detailed description of the compilation process).

It is important to note that because of the adjustments, the compiled map may contain minor errors in the detailed locations of structures, although the general positions should be reliable.

Outcrop patterns in Plate 2 confirm that most E-W-trending ridgelines in the Kura fold-thrust belt are the topographic expression of predominantly south-verging anticlines. Although the spatial resolution of the data was too coarse to allow us to identify surface-breaking faults, the Nalivkin geologic map contains a number of fold-parallel faults within the Kura fold-thrust belt (Plate 2). Most of these faults lie along the southern limbs of the anticlines, although neither fault type nor direction of fault dip is indicated. As with the folds, the number of mapped faults systematically decreases eastward along strike. The structural geometries shown on Plate 2 suggest that these faults are most simply interpreted as south-directed thrusts with hanging-wall anticlines. This conclusion is consistent with previous work identifying the Kura fold-thrust belt as a zone of shallow south-directed thrusting (Tagiyev, 1984; Dotduyev, 1986). The red thrust faults shown on Plate 2 are faults that we identified (i.e., not originally mapped by Nalivkin, 1976) during the construction of the balanced cross sections.

The depth of exposure within the fold-thrust belt decreases eastward along strike. In the west, at ~45°E longitude, the oldest units exposed within the belt include folded Maykopian sediments and volcanics, with Cretaceous rocks to the north (Plate 2). At ~45.5°E the oldest units exposed are Tarkhanian and Chokrakian, with Tarkhanian, Chokrakian, and Sarmatian strata absent east of ~46.5°E. Exposures east of 47°E are predominantly Akchagyl and Apsheron, with exposures of Akchagyl decreasing eastward until they are limited to the cores of anticlines (Plate 2).

It is unlikely that the systematic along-strike variations evident in Plates 1 and 2 result from eastward-increasing burial of the fold-thrust belt. Isopach maps (e.g., Agabekov et al., 1971, 1976; Gasanov and Alyyeva, 2003) confirm that the eastward-narrowing topography (Plate 1) and width of the outcrop belt (Plate 2) both reflect a true along-strike decrease in the cross-strike width of the fold-thrust belt. In particular, Akchagyl and younger sediments do not exhibit abrupt lateral changes in thicknesses outside the confines of the topographic expression of the Kura fold-thrust belt (Fig. DR1 [footnote 1]).

Balanced Cross Sections

Using the data compiled in Plate 2, we constructed two balanced cross sections to evaluate possible along-strike changes in structural

geometry, obtain quantitative estimates of total shortening, and determine the relative importance of variations in rate versus duration of shortening in producing the numerous along-strike variations in the thrust belt described above. Our approach followed methods outlined by Woodward et al. (1989). To constrain the sections, we used (1) the structural geometries determined from our neotectonic mapping, (2) the contacts, unit assignments, and faults reported by Nalivkin (1976), (3) stratigraphic information from our compilation of isopach maps (Azizbekov, 1972; Agabekov et al., 1976; Gasanov and Alyyeva, 2003) and well logs (Azizbekov, 1972; Agabekov and Moshashvili, 1978), and (4) in limited cases, preliminary field observations made during the fall of 2008. Both cross sections are oriented N24°E, perpendicular to the regional strike of the fold-thrust belt. The western section (Fig. 8) is located ~10 km west of the Mingachevir Reservoir, a position that was selected so that the section would pass through an area of dense bedding measurements. The eastern section (Fig. 9) is located between the Turyan and Goy rivers (Plate 2). Bedding data are sparser along this section because the folds are generally mantled by abandoned surfaces in this area. Thus, we located the eastern section to maximize proximity to the available strike-and-dip data and minimize the distance over which relationships exposed along strike would need to be projected into the section.

It is important to note that much of the stratigraphic information in the form of isopach maps and well logs lies outside of the fold-thrust belt itself and thus does not directly constrain subsurface structural geometries. Additionally, we are not aware of available seismic data within the fold-thrust belt. Based on previously published schematic cross sections (e.g., Khain, 1975; Tagiyev, 1984; Dotduyev, 1986; Philip et al., 1989; Sobornov, 1994; Ershov et al., 2003), the relatively shallow depth of exposure throughout the fold-thrust belt, the small plan view distance between exposed structures (~1–10 km), and preliminary field observations, we assume that the Kura fold-thrust belt is characterized by thin-skinned thrusting. As discussed above, there is limited seismicity within the Kura fold-thrust belt, but the few focal mechanisms available suggest that there are events that occur at depths below (~10–20 km) the level we have chosen as our detachment (Fig. 1B; see also Jackson et al., 2002; Tan and Taymaz, 2006). These events suggest that there may be some involvement of deeper structures within the fold-thrust belt, but at present there is even less constraint on the geometry and kinematics of those structures, so we have explicitly not considered them in our analysis.

²GSA Data Repository item 2009154, summary of stratigraphic data and process of map compilation, is available at <http://www.geosociety.org/pubs/ft2009.htm> or by request to editing@geosociety.org.

Specific Assumptions:

- (1) A regional NNE dip of 1° is assumed based on well logs and published structural contour maps.
- (2) These three folds are projected into the line of section from large structures present to the northwest.
- (3) Mid-Miocene age sediments outcrop at the base of the hangingwall of the Mingachevir fault to the west of the line of section.
- (4) On the Nalivkin map there is a small structure depicted here which is not included in the reconstruction. Most places this structure is exposed it places identical units on top of each other, suggesting that there is not significant amounts of displacement on the structure, so its absence should not significantly impact estimates of total shortening.
- (5) The presence of this back thrust is based on preliminary field observations made during the summer of 2008. Preserved geomorphic surfaces on the top and flanks of this surface observed in the field suggest that this is a relatively young structure in the context of the fold-thrust belt as a whole.
- (6) Apsheron age sediments were interpreted as syntectonic, most likely growth strata, but there was insufficient data to attempt to reconstruct this unit along this line of section.
- (7) Structures formed during Steps 2 and 3 could also have formed out of sequence, there is no information that distinguishes between the two possibilities.

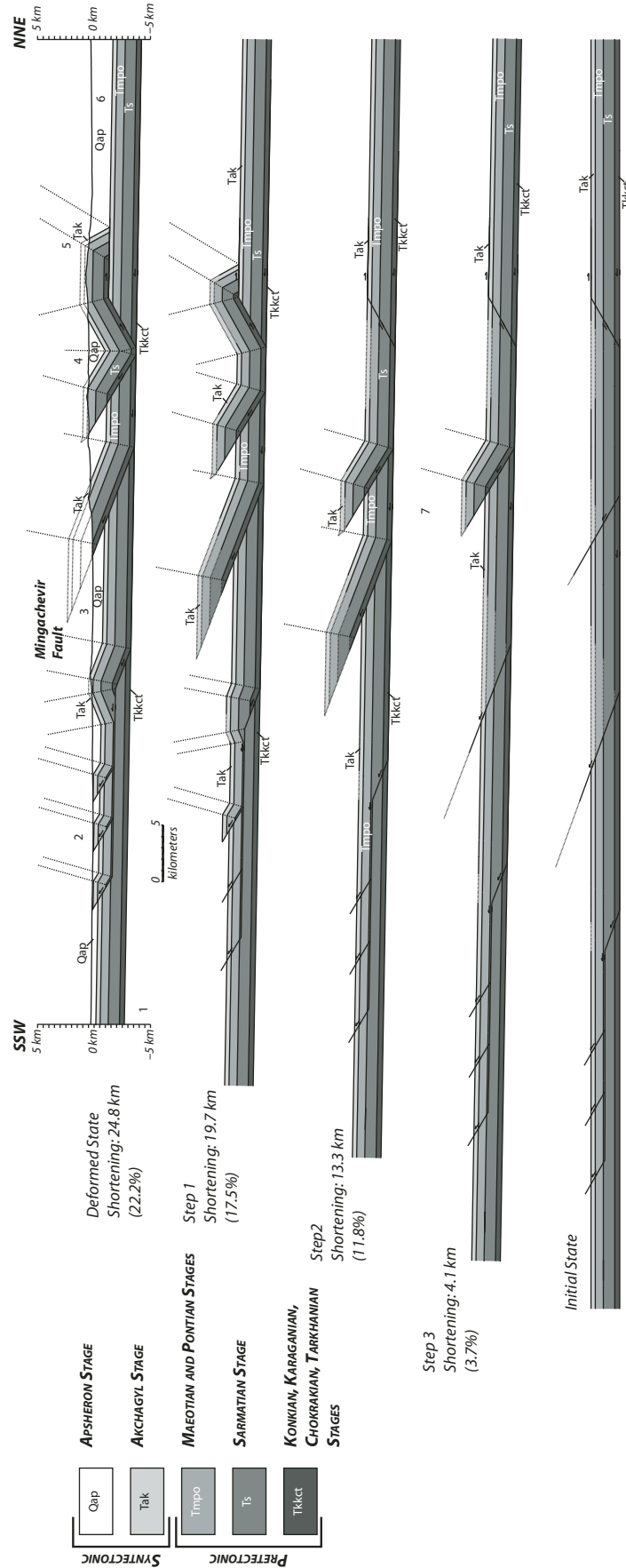


Figure 8. Western balanced cross section; see Plate 2 for location of line of section. Figure shows progressive reconstruction of the section back to an undeformed state highlighting our interpretation of the relative timing of specific structures. Numbers on the cross section refer to specific assumptions made during construction, as explained at the top of the figure. Units are divided into pre-tectonic (constant layer thickness) and syntectonic (variable thickness or nonconformable contacts) deposits, as explained in the text. Note that along this section, both Akchagyl and Apsheron units are classified as syntectonic. For clarity, Quaternary units are not shown.

Specific Assumption:

- (1) Apsheeron age sediments are depicted as growth strata, with deposition beginning shortly before the initiation of folding (represented by the thin deposit preserved on the crest of the main fold).
- (2) The geometry and presence of this large fold is based on exposure to the east of the line of section. It is assumed that these exposures along the line of section are obscured by quaternary deposits. This is believed to be a reasonable assumption based on the presence of the two large drainages on either side of the line of section (the Turyan to the west and the Goy to the east).
- (3) It is clear that this stratigraphy does not exist in this location based on the mapping of Cretaceous rocks exposed in the range front, but there is not sufficient data or constraint to fully incorporate the range front structures into this line of section.
- (4) The sequence of units below the Sarmatian are believed to be the same as elsewhere in the Kura basin (see Figure 4 for clarification) but because they are not exposed, there is little constraint on their thickness in this region of the Kura-Alazani fold-thrust belt.
- (5) We assume that this structure soles into the main detachment below the Greater Caucasus anticlinorium.

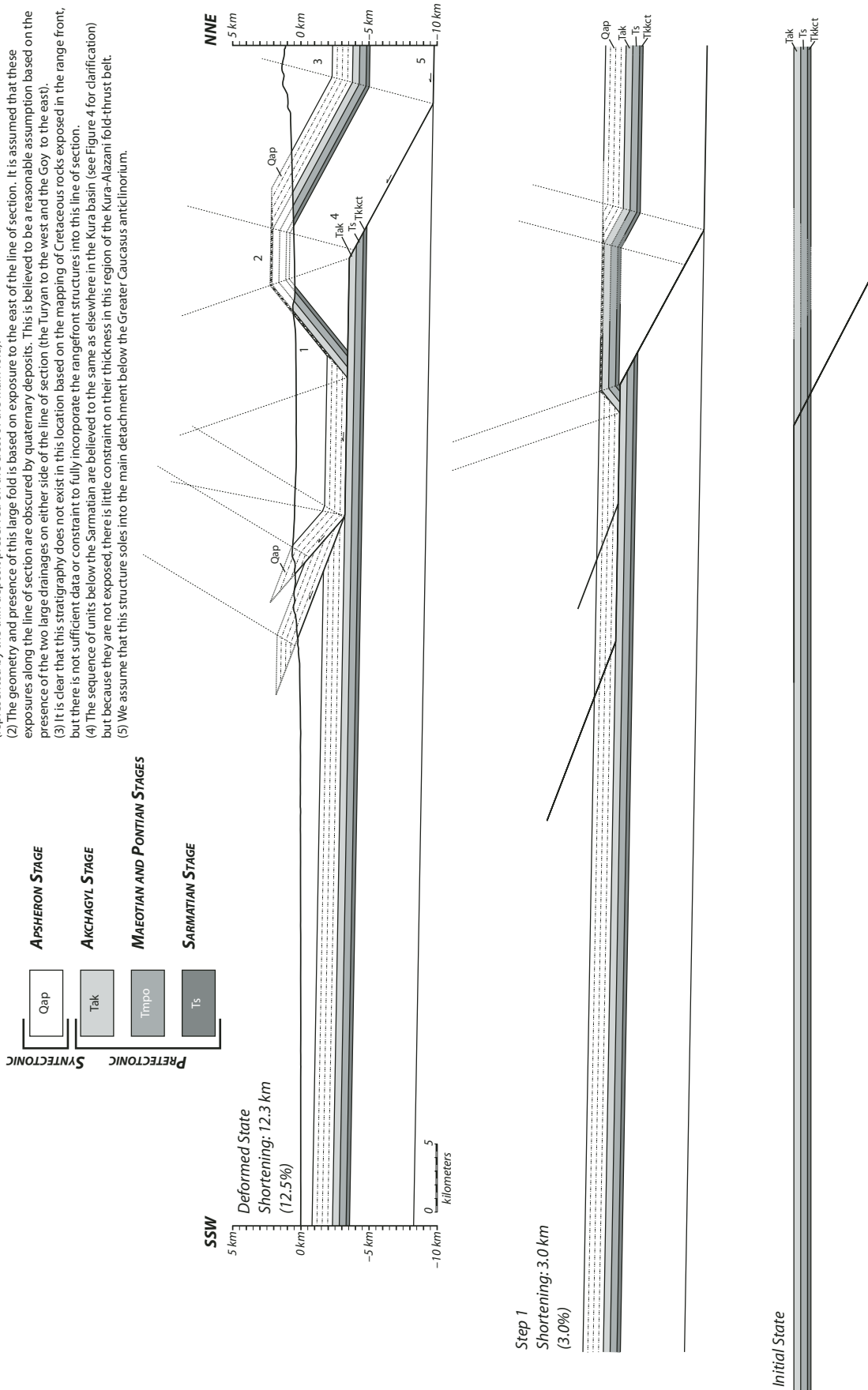


Figure 9. Eastern balanced cross section (location shown on Plate 2) and its progressive reconstruction. In contrast to the western section (Fig. 8), here only Apsheeron appears to be syntectonic. Remaining explanation same as for Figure 8. It is important to note that we do not mean to indicate that the reconstructed stratigraphic sequence continues under the range front of the Greater Caucasus, and we are including this version of the cross section to document the progression by which the cross section was balanced. A more geologically reasonable schematic representation of the interface between the Kura fold-thrust belt and the Greater Caucasus range-front thrust system is presented on Plate 2.

Assuming thin-skinned geometries, our choice of detachment level was guided by previous work and the along-strike variation in depth of exposure evident in Plate 2. Published schematic cross sections listed above illustrate depths to detachment of ~5 km. Khain (1975) suggested that the detachment horizon for the Kura fold-thrust belt lies within Maykopian sediments. Seismic data in the South Caspian also suggest that Maykopian shales serve as the detachment horizon for NW-SE-trending folds offshore of Azerbaijan (Devlin et al., 1999). As Plate 2 indicates, surface exposure of Maykopian and older units are absent throughout much of the Kura fold-thrust belt, thus we conclude that the detachment horizon likely lies within, or stratigraphically above, the Maykopian across most of the belt. We further hypothesize that the detachment shallows eastward along strike, as suggested by the eastward decrease in the depth of exposure.

Along each section we distinguished between sedimentary units with uniform thickness from those with thicknesses that vary locally across individual structures, to identify the layers to balance within the section. In particular, we calculated approximate unit thicknesses exposed along each line of section and also used map patterns to check the conformability of contacts, and in particular whether contacts bounding a given unit were folded similar to, or crosscut, those of underlying layers. Units with contacts that crosscut older folded and/or faulted strata in the geologic map were allowed to vary in thickness across individual structures. Throughout the entire Kura fold-thrust belt, both Apsheron and lower Quaternary units appear to show stratal thinning across individual fold hinges and/or variable thickness on opposite sides of faults with significant stratigraphic throw. In contrast, within the resolution of the data, Akchagyl sediments appeared to crosscut underlying strata in the western part of the fold-thrust belt but were conformable to the east (Plate 2). As we explain in "Timing of Deformation and Evidence for Eastward Propagation," we further suggest that these local variations in stratigraphic thickness and crosscutting relations within the Akchagyl, Apsheron, and Quaternary units can be used to place rough constraints on the timing of deformation within the Kura fold-thrust belt.

For both cross sections, we assumed the simplest possible structural style (i.e., fault-bend folds; Suppe, 1983) and that units without evidence of local thickness variation should maintain constant thickness throughout the line of section. The assumption of fault-bend folding is a simplification, but the available stratigraphic and structural data do not warrant the use of more complex structural geometries such as

fault propagation (Suppe and Medwedeff, 1990) or trishear (Erslev, 1991) folding. As discussed in "Kura and Alazani Basins" and Figure 7, well logs and isopach maps for the Kura Basin suggest that the thickness of Pre-Kimmerian Cenozoic sediments vary along the axis of the Kura Basin, but do not show significant north-south thickness variations, supporting our assumption of constant layer thickness for these units along the lines of section.

Western Section (A–A')

Our reconstruction of the western cross section suggests that this portion of the Kura fold-thrust belt accommodated ~25 km of total shortening or 22% shortening (Fig. 8). Along the line of section, the oldest units exposed are Maeotian-Pontian deposits. However, isolated exposures of underlying Sarmatian and undifferentiated Konkian, Karaganian, Chokrakian, and Tarkhanian deposits occur ~10 and ~20 km west of the section, respectively. Thus, we have placed the detachment horizon for this section within Konkian, Karaganian, Chokrakian, and Tarkhanian strata. Because these exposures lie west of the section line, it is also permissible that the detachment is stratigraphically higher and located within Sarmatian sediments. Jones and Simmons (1996) reported evaporite deposits within exposures of Sarmatian deposits in Armenia, but it is unclear if this evaporite horizon is also present within the Sarmatian deposits of the Kura Basin. If so, it is likely that a detachment horizon would localize on this layer.

One of the main structures along the western section line is the Mingachevir fault (Fig. 8). The original geologic map (Nalivkin, 1976) does not show the fault crossing Quaternary units in the vicinity of the Iori River (i.e., the portion mapped in red on Plate 2). We have interpreted the fault to continue through this area because of the proximity of exposures of Sarmatian and Apsheron deposits to the north and south, respectively, such that ~1 km of section is missing. An alternative interpretation is that this map pattern reflects exposures along the southern limb of an E-W-trending anticline, but there are no strike and dip data to support south-dipping bedding in this area.

Although it has also been suggested that the Mingachevir fault is the product of oblique reverse and sinistral movement (Murtuzayev, 2000), the neotectonic and geologic maps (Plates 1 and 2) show no evidence of significant strike-slip deformation along this structure. Unfortunately, focal mechanisms of earthquakes in the region provide no indication as to the kinematics of the Mingachevir fault. In general, there are limited records of earthquakes within the Kura fold-thrust belt and fewer cal-

culated focal mechanisms. Harvard centroid moment tensor solutions (www.globalcmt.org) for earthquakes near the western termination of the belt are 20–30 km deep and most likely occur on the shallow E-W-striking nodal planes (Fig. 1B). The focal mechanism for the ~16 km deep Agdas earthquake of June 4, 1999 indicates thrusting, but the nodal planes strike N-S, the significance and relation to surface-structure of which is unclear (Tan and Taymaz, 2006). The only indication of strike-slip motion comes from the central Kura Basin, near the so-called 40th parallel shear (Murtuzayev, 2000), with two events suggesting strike-slip and possibly oblique normal faulting, respectively (see Jackson and McKenzie, 1984).

Preliminary field observations from the fall of 2008 suggest that within the western section of the Kura fold-thrust belt there is a backthrust system active along the northern margin of the belt. The neotectonic expression of this structure in the field suggests that it is a relatively young feature, and as such we have interpreted this structure to be part of the most recent stage of shortening (Fig. 8). This observation is also supported by our remotely sensed neotectonic mapping (Plate 1), which contains a band of inferred active structures along the northern margin of the fold-thrust belt.

Eastern Section (B–B')

The western and eastern sections are separated by ~110 km along-strike and appear to record distinct structural histories (Plate 2). We estimate that the eastern section has accommodated ~12 km (12%) total shortening (Fig. 9). The section is dominated by a pair of faults. Along the line of section, only Apsheron and Quaternary sediments are exposed, but ~10 km to the west and east, Kimmerian and Akchagyl strata are exposed in the cores of anticlines. The backthrust system observed in the western regions of the fold-thrust belt does not appear to continue eastward along strike. Much of the shortening estimated in the eastern reconstruction is accommodated in a large hanging-wall anticline, which we interpret as the structural connection between the Greater Caucasus range-front faults and the Kura fold-thrust belt. The geometry and scale of this fold are based mainly on eastward extrapolation of the structural relationships exposed north of Agsu, ~60 km east of the section, where the Kura fold-thrust belt intersects the Greater Caucasus range front. The geometry of the syncline that lies south of the anticline but north of the thrust within the Kura belt is based on extrapolation of structural relationships north of the Mingachevir Reservoir eastward into the line of section. At the north end of the section, the depth to detachment is ~10 km, ramping southward

to a depth of ~3 km at the base of the Apsheron sequence, to form the large ramp-anticline. We interpret the base of the Apsheron sediments as the detachment horizon within the Kura fold-thrust belt because of the lack of exposure of underlying units along both the line of section and westward along strike. Although exposures of Akchagyl and Kimmerian deposits are present to the west along the northern boundary of the Kura fold-thrust belt, we interpret these to result from the westward continuation of the large hanging-wall anticline illustrated in the eastern cross section (Fig. 9). Given the available data and observations, the nature of the connection between the Kura fold-thrust belt and the Greater Caucasus range-front fault system is not clear. Our attempt at reconciling these two structures is most certainly a gross simplification and highlights the need for more detailed assessments of both the age and geologic history of the Greater Caucasus range-front fault system.

Akchagyl sediments do not appear to vary in thickness significantly in the vicinity of the eastern cross section (Fig. 9). This interpretation is based on exposures of Akchagyl to the west and east of the line of section (Plate 2) and is also constrained by isopach maps (e.g., see Fig. 1 of Gasanov and Alyyeva, 2003). In contrast, there appear to be significant thickness variations and onlap relationships in the Apsheron sediments. The ~1500 m thickness of Apsheron sediments exposed along the thrusts in the eastern cross section were taken as the maximum unit thickness and the ~200 m thick exposure along the ridge to the northeast of the section line was taken as the minimum unit thicknesses for the reconstruction of the Apsheron (Fig. 9).

DISCUSSION

Our integrated neotectonic and geologic investigation indicates that the Kura fold-thrust belt results from active shortening along the northern margin of the Arabia-Eurasia collision zone and suggests that total shortening decreases eastward along strike within this belt. At some level, this pattern contrasts with that expected from the GPS-derived velocity field, which indicates shortening rates increase eastward within the same region. Thus, the GPS data suggest that total shortening should be higher in the east than the west for a given amount of time. In the following sections we first discuss constraints on the timing of deformation within the fold-thrust belt, then estimate the relative importance within the Arabia-Eurasia collision of the shortening accommodated by the Kura fold-thrust belt, and finally propose a kinematic model that reconciles the along-strike variation in shortening with geodetic observations.

Timing of Deformation and Evidence for Eastward Propagation

Our key constraints on the initiation of deformation within the fold-thrust belt come from along-strike variations in the degree to which Akchagyl and Apsheron deposits appear concordant or discordant with respect to deformation of underlying units. As we explain below, such variations imply that during the deposition of Akchagyl-aged sediments deformation within the fold-thrust belt had started along the western section but had not yet started in the vicinity of the eastern section. In the following, we discuss specific implications of this interpretation as it relates to the diachroneity of timing of fold-thrust belt initiation along-strike.

We interpreted the Akchagyl as a syntectonic unit in the western reaches of the fold-thrust belt based on its apparent crosscutting of underlying fold structures (Plate 2). This implies that deformation in the vicinity of the western section initiated during or prior to the Akchagyl stage (~3.4–2.5 Ma). Because there are virtually no Kimmerian deposits (Fig. 7) exposed within the fold-thrust belt, it may be that all of the Akchagyl deposits are syntectonic, with deformation beginning during the Kimmerian stage. In this latter case, the maximum initiation age for this portion of the fold-thrust belt is ca. 5.5 Ma. Isopach maps (Agabekov et al., 1976), stratigraphic descriptions (Jones and Simmons, 1996), and thicknesses calculated from Plate 2 suggest that the underlying Maeotian-Pontian sediments show only regional thickness variations, supporting our conclusion that the maximum initiation age for this region of the fold-thrust belt is ca. 5.5 Ma.

In contrast to the western sections of the fold-thrust belt, the Akchagyl appears concordant with respect to folds in the vicinity of the eastern section, suggesting the unit is pre-tectonic in this area (Plate 2), although exposures of Akchagyl sediments in this region are sparse. Along the eastern section, the overlying Apsheron sediments appear to thin across the hinge of the largest anticline but do not appear to show major thickness variations across the southern thrusts, relationships which we interpret to suggest that Apsheron deposition began before the anticline started forming, followed by slip along the thrusts after Apsheron deposition. These relationships suggest thrusting on the main ramp started during the time of Apsheron deposition (1.6–0.7 Ma), with thrusting on the smaller thrusts starting after 0.7 Ma.

Both the neotectonic and geologic records indicate that total shortening within the Kura fold-thrust belt systematically decreases from west to east along strike. Although this pattern

could result from eastward decreasing rates of shortening, the more reasonable explanation is that deformation initiated diachronously along strike, such that the belt has propagated eastward over time. We favor diachronous initiation and eastward propagation for two main reasons: (1) the transition of Akchagyl sediments from syntectonic to pre-tectonic eastward along-strike, and (2) provenance studies (Allen et al., 2003; Hinds et al., 2007) and apatite thermochronology (Král and Gurbanov, 1996; Avdeev and Niemi, 2008) suggesting that the exhumation of the Caucasus has migrated eastward over time.

Preliminary field observations from the fall of 2008 also suggest that there is along-strike variation in the across-strike propagation of the fold-thrust belt. In the vicinity of the Mingachevir Reservoir and to the west, it appears that the fold-thrust belt is propagating both north and south into the Kura and Alazani basins, respectively (Cowgill et al., 2008), whereas in the east, the belt appears to be mainly propagating to the south into the Kura Basin (Forte et al., 2008).

Regional Tectonic Importance

Although the total shortening estimates of 25 and 12 km do not appear large in an absolute sense, comparison of these values to the amount of total Arabia-Eurasia convergence since the early Pliocene indicates that the Kura fold-thrust belt has absorbed ~30%–46% of the total plate convergence over this time interval (Fig. 10). In this analysis, we used Euler poles to compute magnitudes and rates of Arabia-Eurasia relative motion since 5 and 2 Ma, and then compared these results with our independent estimates of the magnitudes and rates of shortening along the western and eastern lines of section, respectively. In so doing, we followed previous workers who have argued that current plate motions within the collision zone can be reliably projected back in time to the last major reorganization within the area, which occurred at ca. 5 Ma (e.g., Westaway, 1994; McQuarrie et al., 2003; Allen et al., 2004). We used ages of 5 and 2 Ma because these represent approximate maximum bounds on the initiation of deformation within the respective sections, and our goal is to compute minimum values for the fraction of total Arabia-Eurasia convergence absorbed by the Kura fold-thrust belt. We explain this approach in more detail below. To evaluate the sensitivity of our analysis to the choice of plate model or reference point, we computed velocities of Arabia relative to Eurasia using three different Euler poles (DeMets et al., 1994; Sella et al., 2002; Reilinger et al., 2006) and two different reference points on the Arabian plate (point 1: 44°E, 35°N; point 2: 45°E, 34°N). At each point we determined the

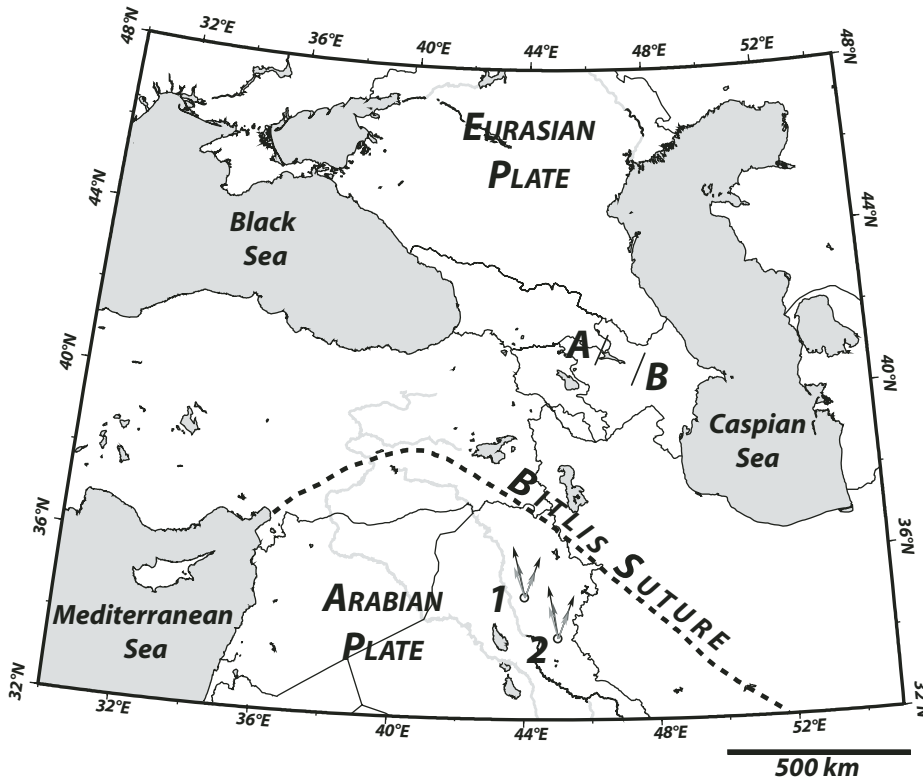


Figure 10. Explanation of calculations used to evaluate percent of total Arabia-Eurasia convergence absorbed by the Kura fold-thrust belt. Map shows locations of western (A) and eastern (B) sections and reference points 1 and 2, which are locations at which motion of Arabia relative to Eurasia was calculated using three different plate models: NUVEL-1A (DeMets et al., 1994, black), an Euler pole derived from a regional global positioning system (GPS) network (Reilinger et al., 2006, gray), and REVEL 2000 (Sella et al., 2002, light gray). Northwest-pointing arrows at these points indicate total velocity. Those pointing north-east show only the N20°E component of motion, which is perpendicular to the Kura and Greater Caucasus. Chart at bottom of figure reports rates and magnitudes of shortening. Numbers above the tables are for the Kura fold-thrust belt as independently determined from our balanced cross sections and analysis of stratigraphic data. Numbers within table show rates and magnitudes of Arabia relative to Eurasia computed for past 5 and 2 Ma for the western and eastern sections, respectively. To compute percentage of total Arabia-Eurasia convergence accommodated by Kura fold-thrust belt, we compared the shortening values from the thrust belt with total magnitudes of N20°E component of motion of Arabia relative to Eurasia as computed from plate models.

WESTERN CROSS SECTION (A)

TOTAL SHORTENING ESTIMATE: ~25 km APPROXIMATE INITIATION AGE: 5 Ma IMPLIED SHORTENING RATE: 5 mm/a

REFERENCE SITE 1: 44°E, 35°N

MODEL	AZIMUTH	VELOCITY	N20E CONVERGENCE RATE	N20E CONVERGENCE SINCE 5 MA	PERCENTAGE ACCOMMODATED BY KURA FOLD-THRUST BELT
NUVEL-1A	-13°	26 mm/a	22 mm/a	110 km	22%
REILINGER	-10°	18 mm/a	16 mm/a	78 km	32%
REVEL 2000	-20°	16 mm/a	13 mm/a	63 km	40%

REFERENCE SITE 2: 45°E, 34°N

MODEL	AZIMUTH	VELOCITY	N20E CONVERGENCE RATE	N20E CONVERGENCE SINCE 5 MA	PERCENTAGE ACCOMMODATED BY KURA FOLD-THRUST BELT
NUVEL-1A	-11°	27 mm/a	23 mm/a	115 km	22%
REILINGER	-7°	19 mm/a	17 mm/a	85 km	30%
REVEL 2000	-16°	17 mm/a	14 mm/a	70 km	36%

EASTERN CROSS SECTION (B)

TOTAL SHORTENING ESTIMATE: ~12 km APPROXIMATE INITIATION AGE: 2 Ma IMPLIED SHORTENING RATE: 6 mm/a

REFERENCE SITE 1: 44°E, 35°N

MODEL	AZIMUTH	VELOCITY	N20E CONVERGENCE RATE	N20E CONVERGENCE SINCE 2 MA	PERCENTAGE ACCOMMODATED BY KURA FOLD-THRUST BELT
NUVEL-1A	-13°	26 mm/a	22 mm/a	44 km	27%
REILINGER	-10°	18 mm/a	16 mm/a	31 km	39%
REVEL 2000	-20	16 mm/a	13 mm/a	26 km	46%

REFERENCE SITE 2: 45°E, 34°N

MODEL	AZIMUTH	VELOCITY	N20E CONVERGENCE RATE	N20E CONVERGENCE SINCE 2 MA	PERCENTAGE ACCOMMODATED BY KURA FOLD-THRUST BELT
NUVEL-1A	-11°	27 mm/a	23 mm/a	46 km	27%
REILINGER	-7°	19 mm/a	17 mm/a	34 km	35%
REVEL 2000	-16°	17 mm/a	14 mm/a	27 km	46%

N20°E component of motion of Arabia relative to Eurasia because this direction is roughly perpendicular to the regional strike of both the Kura fold-thrust belt and the Greater Caucasus. In all three plate models Arabia rotates counterclockwise relative to Eurasia about an Euler pole in the eastern Mediterranean, but they differ in terms of rotation rate and Euler pole location, as well as the methods by which the poles were determined. For example, the NUVEL-1A model (DeMets et al., 1994) is based on paleomagnetic data and oceanic spreading rates over the past 3 Ma. In contrast, the REVEL 2000 model (Sella et al., 2002) is based on a global plate velocity solution from space geodesy, whereas the Reilinger et al. (2006) model is based on regional geodetic measurements within the Arabia-Eurasia collision.

Along the western section (A–A'), we computed total Arabia-Eurasia convergence since 5 Ma because the lack of Kimmerian sediments in the area permits deformation to have initiated as early as this time. In addition, the apparent absence of local thickness variations within the upper Miocene Maotian-Pontian strata makes it unlikely that major shortening within this sector of the fold-thrust belt would have initiated significantly prior to ca. 5 Ma. Combining the 5 Ma initiation age with the ~25 km total shortening estimate suggests a rate of ~5 mm/a. Depending on the plate velocity model used, the ~25 km of total shortening along A–A' represents 22% to 40% of the total N20°E component of Arabian convergence relative to Eurasia since 5 Ma (Fig. 10). The NUVEL-1A model has been shown to report anomalously fast rates (e.g., Sella et al., 2002), and removing it from consideration suggests that the western section could account for 30%–40% of total Arabia-Eurasia convergence since 5 Ma.

Along the eastern section (B–B'), we computed total Arabia-Eurasia convergence since 2 Ma because our stratigraphic analysis suggests deformation did not initiate in this area until at least the timing of Apsheron deposition (0.7–1.6 Ma, Fig. 7). In this case, the ~12 km of total shortening along B–B' represents between 27% and 46% of total Arabia-Eurasia convergence since 2 Ma, with the estimates converging on 35%–46%, if the NUVEL-1A model is excluded as above. For the eastern section, combining the shortening estimate (~12 km) with the stratigraphically constrained initiation age of 2 Ma implies a rate of 6 mm/a.

Although the above analysis indicates that the Kura fold-thrust belt has played a crucial role in accommodating Arabia-Eurasia convergence since the early Pliocene, these calculations are subject to uncertainties. For example, if our total shortening estimates from the balanced sections

are too high, then both the percentage of total Arabia-Eurasia convergence and the implied shortening rates calculated for the Kura fold-thrust belt will be too high. Likewise, if shortening initiated earlier than ca. 5 Ma within the fold-thrust belt, then again both the percentage of total convergence and the implied shortening rates will be too high. As described earlier, there are additional and potentially large uncertainties involved in the correlation of regional stages to absolute ages. Finally, there are also uncertainties associated with extrapolation of the plate models back to 5 Ma.

Geologic versus GPS Deformation

If we assume that the average geologic rates implied by the balanced sections are representative of current shortening rates within the Kura fold-thrust belt and then compare those to the magnitudes of the GPS-derived rates of convergence and their along-strike variation, there is not an immediate disconnect between the two; however, inconsistencies develop if we attempt to extrapolate the rates backward through time. Our balanced sections and stratigraphic relationships imply average shortening rates of 5 mm/a, and 6 mm/a for the western and eastern sections, respectively (Fig. 10). As mentioned above, GPS stations within the Kura Basin and Lesser Caucasus move toward N20°E relative to Eurasia, with velocities that increase systematically eastward along strike (Reilinger et al., 2006). Along the western and eastern sections, these geodetic rates are ~10 and 12 mm/a, respectively (Fig. 2). Thus, if we assume the average geologic rates are also representative of the current rates of shortening within the Kura fold-thrust belt, this would imply that convergence in this region is equally partitioned between the Greater Caucasus and the Kura fold-thrust belt.

If the current convergence rates can be reliably extrapolated back to ca. 5 Ma (e.g., Westaway, 1994; McQuarrie et al., 2003; Allen et al., 2004) and our estimation of along-strike variation of initiation ages within the fold-thrust belt is correct, then we can assume that at roughly 2 Ma, the eastern section of the Kura fold-thrust belt was not accommodating significant amounts of shortening, implying that at this time, the Greater Caucasus were accommodating the full ~12 mm/a of convergence. However, within the Greater Caucasus, we see a similar eastward decrease in proxies for total shortening (i.e., lower elevations, smaller plan view width of the range, and younger ages for exhumation events) which is potentially incompatible with idea of the Greater Caucasus accommodating the excess convergence (N. Niemi, 2009, personal commun.).

One obvious potential explanation for these differences is the possibility that the GPS velocity field does not accurately reflect the recent (i.e., post-5 Ma) tectonics of the area. For example, the velocity field may contain post-seismic transient strains due to recent large earthquakes in the region, such as the M 6.9 1988 Spitak earthquake in Armenia (Philip et al., 1992) or the M 7.0 1991 Racha earthquake in Georgia (Triep et al., 1995). Likewise, recent structural reorganization within the system could also cause the GPS and geologic deformation fields to disagree. Similar discrepancies between GPS and geologically derived rates of deformation have been identified in a number of other regions (e.g., Bennett et al., 2004; Oskin and Iriondo, 2004; Brown et al., 2005; Chevalier et al., 2005; Frankel et al., 2007a; Frankel et al., 2007b; Oskin et al., 2007; Thatcher, 2007).

However, an alternative explanation is also possible that potentially reconciles the GPS and geologic deformation fields with inferred east-directed propagation of the Kura fold-thrust belt and Greater Caucasus (Fig. 11). For the current GPS velocity field to accurately reflect strain in the region since 5 Ma, total shortening must be larger in the east than the west. Such eastward-increasing total shortening can be reconciled with the eastward-decreasing shortening in the Kura fold-thrust belt, if the excess convergence was absorbed by an additional structure(s) in the region. The model must also explain the apparent eastward propagation of the Greater Caucasus (Allen et al., 2003) and the corresponding eastward decrease in the topographic width and height of the range toward the Apsheron Peninsula.

In the proposed kinematic model (Fig. 11), convergence between the Lesser and Greater Caucasus increases from west to east, as indicated by the GPS velocity field. Initially, there is a remnant of oceanic crust from the Greater Caucasus backarc basin along the southern margin of what will become the Greater Caucasus as suggested by Zonenshain and Le Pichon (1986). All convergence in the region is initially accommodated along the Greater Caucasus range-front fault system, growing the Greater Caucasus in the west and subducting remnant oceanic crust in the east. As this remnant oceanic crust is consumed, convergence is accommodated by shortening of the upper plate, growing and propagating the Greater Caucasus eastward over time. Concurrently, in the west, deformation begins to propagate southward into the foreland, forming the Kura fold-thrust belt. Migration of deformation into the foreland may be in response to the interior of the Greater Caucasus reaching a critical height, as suggested by Allen et al. (2004). As slip transfers to the Kura fold-thrust belt in the west, shortening within the corresponding

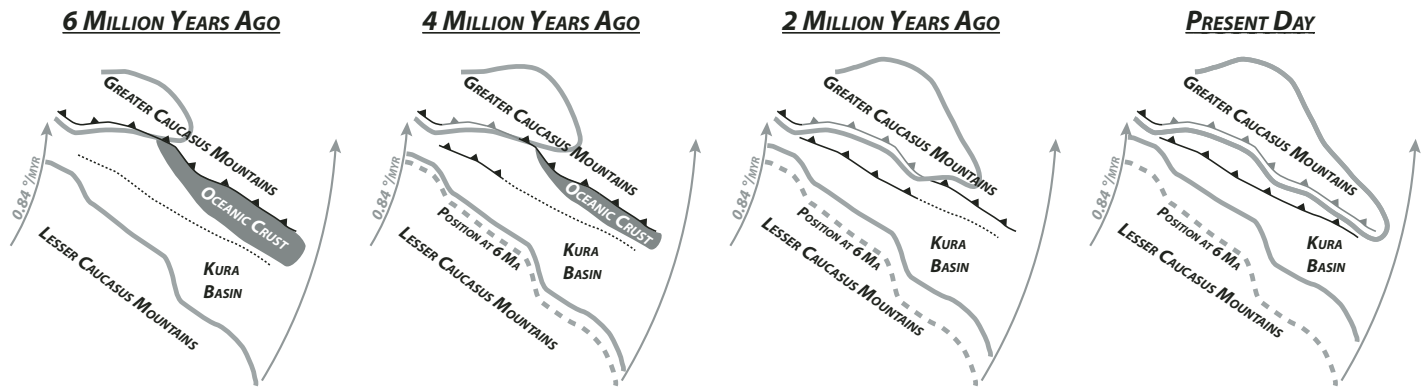


Figure 11. Kinematic model of progressive eastward propagation of the Kura fold-thrust belt and Greater Caucasus. This model reconciles eastward-decreasing magnitudes and timing of deformation within the Kura fold-thrust belt and the Greater Caucasus with eastward-increasing rates of total convergence as seen in the global positioning system (GPS) velocity field. See text for discussion. Lesser Caucasus rotate counterclockwise about a pole in the eastern Black Sea at $0.84^\circ/\text{Ma}$ relative to the Greater Caucasus, as indicated by recent GPS data (Reilinger et al., 2006). Barbed lines schematically represent the Greater Caucasus range-front fault system and the Kura fold-thrust belt. Dashed black line indicates future location of Kura fold-thrust belt. Thrusts shown in black are active; those in gray have reduced slip rates.

area of the Greater Caucasus slows. Farther east, as the oceanic remnant is completely subducted, the Greater Caucasus continue to propagate eastward toward the Apsheron Peninsula. Subsequent eastward propagation of the Kura fold-thrust belt is matched by a corresponding drop in the rate of shortening within the Greater Caucasus. Thus, according to this model, the formation and eastward propagation of both the Greater Caucasus and Kura fold-thrust belt is the product of the progressive eastward consumption of a relict ocean basin.

Though not illustrated in this schematic model, the West Caspian Fault (Fig. 1) must function as a right-lateral transform to isolate the remnant oceanic crust subducted beneath the Greater Caucasus from the oceanic crust that remains in the South Caspian Basin. This would further suggest the presence of what is essentially a triple junction between the faults bounding the southern margin of the Greater Caucasus, the West Caspian Fault, and the Apsheron Sill.

CONCLUSIONS

We draw several conclusions from our neotectonic mapping of the Kura fold-thrust belt along the northern margin of the Kura Basin and southern margin of the Greater Caucasus.

- (1) The Kura fold-thrust belt comprises south-vergent folds that trend roughly parallel to the Greater Caucasus and deform Tertiary through Quaternary sediments.
- (2) Structures within this belt appear to be active, as indicated by folded abandoned surfaces of probable Quaternary age, ephemeral

geomorphic features such as wind gaps, and anomalous drainage patterns that are characteristic of active fold growth.

- (3) The belt shows systematic along-strike variation in both structural complexity and topography, with more structures, larger cross-strike width, and greater volume in the western portion of the belt relative to the east. The simplest interpretation for these variations is that total shortening decreases eastward along strike.

By integrating our neotectonic observations with a new synthesis of published information regarding the regional stratigraphy and geology, we were able to construct two balanced cross sections across the Kura fold-thrust belt. Several additional conclusions can be drawn from this analysis of the regional bedrock geology.

- (4) Deeper stratigraphic levels are exposed in the western part of the belt than in the east, supporting the conclusion drawn from our neotectonic mapping that structural complexity decreases eastward along strike. Isopach maps and bore-hole data together indicate that these along-strike variations do not result from greater burial of the fold-thrust belt in the east than in the west. We interpret the along-strike variation in exposed stratigraphic depth to result from an eastward-decreasing depth to detachment within the fold-thrust belt.
- (5) Our balanced cross sections indicate both a greater magnitude and earlier onset of shortening in the west than in the east. Specifically, total shortening along the western section is ~ 25 km ($\sim 22\%$), in contrast to

~ 12 km (12%) along the eastern section. Local variations in unit thickness across structures and depositional contacts that crosscut underlying layers together suggest that deformation initiated before or during Akchagyl time (3.4–1.6 Ma) along the western section but not until prior to the Apsheron (1.6–0.7 Ma) in the east. Thus, we interpret the along-strike variation in total shortening to result from eastward propagation and diachronous initiation of shortening within the Kura fold-thrust belt.

- (6) The Kura fold-thrust belt appears to be a major structural system within the Arabia-Eurasia collision zone. Comparison of our shortening estimates with total magnitudes of $N20^\circ E$ convergence within the collision as derived from global and regional plate models suggests that the Kura fold-thrust belt has accommodated between 30% and 45% of total Arabia-Eurasia convergence within the Caucasus since 5 Ma.
- (7) To reconcile the geologic record of eastward-decreasing total shortening and initiation age within the Kura fold-thrust belt with GPS velocities indicating eastward-increasing convergence rates, we propose that eastward propagation of the fold-thrust belt is intricately coupled with the eastward growth and propagation of the Greater Caucasus and the closing of a remnant ocean basin that once existed between the two.

The results of this study also suggest the importance of localization in accommodating convergence, even in relatively young orogenic systems. The focusing of Arabia-Eurasia convergence within both the Greater Caucasus

and Kura fold-thrust belt has many implications for our understanding of mechanisms by which first-order structures develop and evolve in continent-continent collisions.

ACKNOWLEDGMENTS

In developing the ideas presented here, we benefited from conversations with Nathan Niemi, Ibrahim Murtuzayev, Rauf Nadirov, Doug Burbank, Ryan Gold, Howard Day, and Sean Mulcahy. Sarah Roeske and Magali Billen provided helpful comments on an early version of this work. Reviews by Mark Allen, Damien Dhont, and Douwe van Hinsbergen contributed greatly to the clarity and quality of this paper. We are indebted to the makers of the Generic Mapping Tools (Wessel and Smith, 1995) and to Richard Allmendinger for making Fault/Fold version 5.4 available. This project was supported by National Aeronautics and Space Administration grant EOS/03-0663-0306 and National Science Foundation grant EAR-0810285. Additional funding for Adam Forte came from the University of California, Davis, Department of Geology Durrell Fund.

REFERENCES CITED

- Adamia, S., Lordkipandize, M.B., and Zakariadze, G.S., 1977, Evolution of an active continental margin as exemplified by the alpine history of the Caucasus: *Tectonophysics*, v. 40, p. 183–199, doi: 10.1016/0040-1951(77)90065-8.
- Adamia, S., Asanidze, B.Z., Gambashidze, R.A., Nadareyshivili, G.S., and Thoa, N.T.K., 1979, Paleomagnetism of Upper Cretaceous rocks of Southern Georgia and its geologic interpretation: *International Geology Review*, v. 22, no. 11, p. 1241–1256.
- Adamia, S., Akhvlediani, K.T., Kilasonia, V.M., Nairn, A.E.M., Papava, D., and Patton, D.K., 1992, Geology of the Republic of Georgia: A review: *International Geology Review*, v. 34, no. 5, p. 447–476.
- Agabekov, M.G., and Moshashvili, A.B., 1978, Kyurdamir-Saatly buried uplift of the Kura Basin, an integral part of the Lesser Caucasus geosyncline in Cretaceous time: *Doklady of the National Academy of Sciences of the Union of Soviet Socialist Republics*, v. 232, p. 120–122.
- Agabekov, M.G., Azizbekov, S.A., Akhmedbejli, F.S., Gadzhiev, T.G., Grigor'nc, B.V., Mamedov, A.V., and Shikalibeily, E.S., 1971, Tectonic schema of Azerbaijan SSR (In Russian): Ministry of Geology, Union of Soviet Socialist Republics, scale 1:1,000,000.
- Agabekov, M.G., Kerimov, K.M., Moshashvili, A.B., and Khain, V.Y., 1976, New data on the structure of the central part of the Kura trough: *Geotectonics*, v. 10, p. 350–354.
- Allen, M.B., and Armstrong, H.A., 2008, Arabia-Eurasia collision and the forcing of mid-Cenozoic global cooling: *Palaeogeography, Palaeoclimatology, Palaeoecology*, v. 265, p. 52–58, doi: 10.1016/j.palaeo.2008.04.021.
- Allen, M.B., Jones, S., Ismail-Zadeh, A., Simmons, M., and Anderson, L., 2002, Onset of subduction as the cause of rapid Pliocene-Quaternary subsidence in the South Caspian basin: *Geology*, v. 30, no. 9, p. 775–778, doi: 10.1130/0091-7613(2002)030<0775:OOSATC>2.0.CO;2.
- Allen, M.B., Vincent, S.J., Alsop, G.I., Ismail-Zadeh, A., and Flecker, R., 2003, Late Cenozoic deformation in the South Caspian region: Effects of a rigid basement block within a collision zone: *Tectonophysics*, v. 366, p. 223–239, doi: 10.1016/S0040-1951(03)00098-2.
- Allen, M.B., Jackson, J., and Walker, R., 2004, Late Cenozoic reorganization of the Arabia-Eurasia collision and the comparison of short-term and long-term deformation rates: *Tectonics*, v. 23, TC2008, doi: 10.1029/2003TC001530.
- Allmendinger, R.W., Reilinger, R., and Loveless, J., 2007, Strain and rotation rate from GPS in Tibet, Anatolia, and the Altiplano: *Tectonics*, v. 26, TC3013, doi: 10.1029/2006TC002030.
- Asanidze, B.Z., and Pecherskiy, D.M., 1979, Paleomagnetic studies of Jurassic rocks in Georgia and the northern Caucasus: *Izvestiya: Physics of the Solid Earth*, v. 15, no. 10, p. 736–747.
- Avdeev, B., and Niemi, N.A., 2008, Constraints on the rates and timing of exhumation of the Greater Caucasus from low-temperature thermochronology: *Eos (Transactions, American Geophysical Union)*, v. 89, no. 53.
- Axen, G.J., Lam, P.S., Grove, M., Stockli, D.F., and Hassan-zadeh, J., 2001, Exhumation of the west-central Alborz Mountains, Iran, Caspian subsidence, and collision-related tectonics: *Geology*, v. 29, no. 6, p. 559–562, doi: 10.1130/0091-7613(2001)029<0559:EOTWCA>2.0.CO;2.
- Azizbekov, S.A., 1972, Azerbaijan SSR (in Russian), *Geology of the USSR: Moscow, Nauka*, p. 433.
- Banks, C.J., Robinson, A.G., and Williams, M.P., 1997, Structure and regional tectonics of the Achara-Trialet fold belt and the adjacent Rioni and Karli foreland basins, Republic of Georgia, in Robinson, A.G., ed., *Regional and petroleum geology of the Black Sea and surrounding region: American Association of Petroleum Geologists Memoir*, p. 331–346.
- Barka, A., 1992, The North Anatolian fault zone: *Annales Tectonicae*, v. 6 (Special Issue: Supplement to v. 6), p. 164–195.
- Bazhenov, M.L., and Burtman, V.S., 1989, Paleomagnetism of Upper Cretaceous rocks from the Caucasus and its implications for tectonics, in Sengor, A.M.C., ed., *Tectonic evolution of the Tethyan Region: Kluwer Academic Publishing*, p. 217–239.
- Bazhenov, M.L., and Burtman, V.S., 2002, Eocene paleomagnetism of the Caucasus (southwest Georgia): Oroclinal bending in the Arabian syntaxis: *Tectonophysics*, v. 344, p. 247–259, doi: 10.1016/S0040-1951(01)00189-5.
- Beaumont, C., Fullsack, P., and Hamilton, J., 1991, Erosional control of active compressional orogens, in McClay, K.R., ed., *Thrust tectonics: New York, Chapman Hall*, p. 1–18.
- Bennett, R.A., Friedrich, A.M., and Furlong, K.P., 2004, Codependent histories of the San Andreas and San Jacinto fault zones from inversion of fault displacement rates: *Geology*, v. 32, no. 11, p. 961–964, doi: 10.1130/G20806.1.
- Berberian, M., 1983, The southern Caspian: A compressional depression floored by a trapped, modified oceanic crust: *Canadian Journal of Earth Sciences*, v. 20, p. 163–183.
- Berberian, M., and King, G.C.P., 1981, Towards a paleogeography and tectonic evolution of Iran: *Canadian Journal of Earth Sciences*, v. 18, p. 210–265, doi: 10.1139/e81-163.
- Berberian, M., and King, G.C.P., 1997, Seismic sources of the Transcaucasian historical earthquakes, in Giardini, D., and Balassanian, S., eds., *Historical and prehistorical earthquakes in the Caucasus: Kluwer Academic Publishers*, p. 233–311.
- Berberian, M., and Yeats, R.S., 1999, Patterns of historical earthquake rupture in the Iranian Plateau: *Bulletin of the Seismological Society of America*, v. 89, p. 120–139.
- Bernardin, T., Cowgill, E., Gold, R.D., Hamann, B., Kreylos, O., and Schmitt, A., 2006, Interactive mapping on 3-D terrain models: *Geochemistry Geophysics Geosystems*, v. 7, no. 10, Q10013, doi: 10.1029/2006GC001335.
- Borisov, A.A., 1965, *Climates of the U.S.S.R.: Edinburgh and London, Oliver and Boyd*.
- Brown, E.T., Molnar, P., and Bourles, D.L., 2005, Comment on “Slip-rate measurements on the Karakorum fault may imply secular variations in fault motion”: *Science*, v. 309, p. 1326b–1326c, doi: 10.1126/science.1112508.
- Bull, W.B., and McFadden, L.D., 1977, Tectonic geomorphology north and south of the Garlock fault, California, in Doehring, D.O., ed., *Geomorphology in arid regions: Binghamton, New York, State University of New York at Binghamton*, p. 115–138.
- Burbank, D., and Anderson, R.S., 2001, *Tectonic geomorphology: Malden, Massachusetts, Blackwell Publishing*, 274 p.
- Burbank, D., Meigs, A., and Brozovic, N., 1996, Interactions of growing folds and coeval depositional systems: *Basin Research*, v. 8, p. 199–223, doi: 10.1046/j.1365-2117.1996.00181.x.
- Burbank, D., McLean, J.K., Bullen, M., Abdrakhmatov, K.Y., and Miller, M.M., 1999, Partitioning of intermontane basins by thrust-related folding, Tien Shan, Kyrgyzstan: *Basin Research*, v. 11, p. 75–92, doi: 10.1046/j.1365-2117.1999.00086.x.
- Chevalier, M.-L., Ryerson, F.J., Tapponnier, P., Finkel, R.C., Van Der Woerd, J., Haibing, L., and Qing, L., 2005, Slip-rate measurements on the Karakorum fault may imply secular variations in fault motion: *Science*, v. 307, p. 411–414, doi: 10.1126/science.1105466.
- Copley, A., and Jackson, J., 2006, Active tectonics of the Turkish-Iranian Plateau: *Tectonics*, v. 25, TC6006, doi: 10.1029/2005TC001906.
- Cowgill, E., Forte, A.M., Murtuzayev, I., and Kangarli, T., 2008, Localization of Pliocene to present Arabia-Eurasia convergence in the Kura fold-thrust belt, Azerbaijan: *Eos (Transactions, American Geophysical Union)*, v. 89, no. 53.
- Dahlen, F.A., 1990, Critical taper model of fold-and-thrust belts and accretionary wedges: *Annual Review of Earth and Planetary Sciences*, v. 18, p. 55–99, doi: 10.1146/annurev.earth.18.050190.000415.
- Dahlen, F.A., and Suppe, J., 1988, Mechanics, growth, and erosion of mountain belts, in Clark Jr., S.P., Burchfiel, B.C., and Suppe, J., eds., *Processes in continental lithospheric deformation: Geological Society of America Special Paper*, p. 161–178.
- Davis, D., Suppe, J., and Dahlen, F.A., 1983, Mechanics of fold-and-thrust belts and accretionary wedges: *Journal of Geophysical Research*, v. 88, no. B2, p. 1153–1172, doi: 10.1029/JB088iB02p01153.
- DeMets, C., Gordon, R.G., Argus, D.F., and Stein, S., 1994, Effect of recent revisions to the geomagnetic reversal time scale on estimates of current plate motions: *Geophysical Research Letters*, v. 21, no. 20, p. 2191–2194, doi: 10.1029/94GL02118.
- Devlin, W.J., Cogswell, J.M., Gaskins, G.M., Isaken, G.H., Pither, D.M., Puls, D.P., Stanley, K.O., and Wall, G.R.T., 1999, South Caspian Basin: Young, cool, and full of promise: *GSA Today*, v. 9, no. 7, p. 1–9.
- Dewey, J.F., Hempton, M.R., Kidd, W.S.F., Saroglu, F., and Sengor, A.M.C., 1986, Shortening of continental lithosphere: the neotectonics of Eastern Anatolia—A young collision zone, in Coward, M.P., and Ries, A.C., eds., *Collision tectonics: The Geological Society of London Special Publication*, p. 3–36.
- Dhont, D., and Chorowicz, J., 2006, Review of the neotectonics of the Eastern Turkish-Armenian Plateau by geomorphic analysis of digital elevation model imagery: *International Journal of Earth Sciences*, v. 95, p. 34–49, doi: 10.1007/s00531-005-0020-3.
- Dotduyev, S.I., 1986, Nappe structure of the Greater Caucasus range: *Geotectonics*, v. 20, no. 5, p. 420–430.
- Ershov, A.V., Brunet, M.-F., Nikishin, A.M., Bolotov, S.N., Nazarevich, B.P., and Korotae, M.V., 2003, Northern Caucasus basin: Thermal history and synthesis of subsidence models: *Sedimentary Geology*, v. 156, p. 95–118, doi: 10.1016/S0037-0738(02)00284-1.
- Erslev, E.A., 1991, Trishear fault-propagation folding: *Geology*, v. 19, p. 617–620, doi: 10.1130/0091-7613(1991)019<0617:TFFP>2.3.CO;2.
- Farr, T.G., Rosen, P.A., Caro, E., Crippen, R., Duren, R., Hensley, S., Kobrick, M., Paller, M., Rodriguez, E., Roth, L., Seal, D., Shaffer, S., Shimada, J., Umland, J., Werner, M., Oskin, M., Burbank, D., and Alsdorf, D., 2007, The shuttle radar topography mission: *Reviews of Geophysics*, v. 45, p. 1–33, doi: 10.1029/2005RG000183.
- Forte, A.M., Cowgill, E., Murtuzayev, I., and Kangarli, T., 2008, Structural styles of active shortening within the Kura fold-thrust belt: Insights from the Qaramaryam fold, Azerbaijan: *Eos (Transactions, American Geophysical Union)*, v. 89, no. 53.
- Frankel, K.L., and Dolan, J.F., 2007, Characterizing arid regional alluvial fan surface roughness with airborne laser swath mapping digital topographic data: *Journal of Geophysical Research*, v. 112, F02025, doi: 10.1029/2006JF000644.

- Frankel, K.L., Brantley, K.S., Dolan, J.F., Finkel, R.C., Klinger, R.E., Knott, J.R., Machette, M.N., Owen, L.A., Philips, F.M., Slate, J.L., and Wernicke, B.P., 2007a, Cosmogenic ¹⁰Be and ³⁶Cl geochronology of offset alluvial fans along the northern Death Valley fault zone: Implications for transient strain in the eastern California shear zone: *Journal of Geophysical Research*, v. 112, B06407, doi: 10.1029/2006JB004350.
- Frankel, K.L., Dolan, J.F., Finkel, R.C., Owen, L.A., and Hoeft, J.S., 2007b, Spatial variations in slip rate along the Death Valley-Fish Lake Valley fault system determined from LiDAR topographic data and cosmogenic ¹⁰Be geochronology: *Geophysical Research Letters*, v. 34, L18303, doi: 10.1029/2007GL030549.
- Gamkrelidze, I.P., 1986, Geodynamic evolution of the Caucasus and adjacent areas in alpine time: *Tectonophysics*, v. 127, p. 261–277, doi: 10.1016/0040-1951(86)90064-8.
- Gasanov, T.A., and Alyyeva, S.G., 2003, Stratigraphy of sediments of Akchagyl and Apsheon in foothills of southeast part of Lesser Caucasus: *Petroleum Geology*, v. 37, p. 23–30.
- Golonka, J., 2004, Plate tectonic evolution of the southern margin of Eurasia in the Mesozoic and Cenozoic: *Tectonophysics*, v. 381, p. 235–273, doi: 10.1016/j.tecto.2002.06.004.
- Golonka, J., 2007, Geodynamic evolution of the South Caspian Basin, in Yilmaz, P.O., and Isaken, G.H., eds., *Oil and gas of the Greater Caspian Area: American Association of Petroleum Geologists, Studies in Geology*, p. 17–41.
- Gradstein, F.M., Ogg, J.G., and Smith, A.G., 2004, *A geological time scale 2004*: Cambridge University Press, 589 p.
- Guest, B., Axen, G.J., Lam, P.S., and Hassanzadeh, J., 2006, Late Cenozoic shortening in the west-central Alborz Mountains, northern Iran, by combined conjugate strike-slip and thin-skinned deformation: *Geosphere*, v. 2, no. 1, p. 35–52, doi: 10.1130/GES00019.1.
- Hafkenscheid, E., Wortel, M.J.R., and Spakman, W., 2006, Subduction history of the Tethyan region derived from seismic tomography and tectonic reconstructions: *Journal of Geophysical Research*, v. 111, B080401, doi: 10.1029/2005JB003791.
- Hempton, M.R., 1987, Constraints on Arabian plate motion and extensional history of the Red Sea: *Tectonics*, v. 6, p. 687–705, doi: 10.1029/TC006i006p0687.
- Hinds, D.J., Simmons, M., Allen, M.B., and Aliyeva, E., 2007, Architecture variability in the Pereriva and Balakhany Suites of the Neogene Productive Series, Azerbaijan: Implications for reservoir quality, in Yilmaz, P.O., and Isaken, G.H., eds., *Oil and gas of the Greater Caspian area: American Association of Petroleum Geologists, Studies in Geology*, p. 87–107.
- Hirano, A., Welch, R., and Lang, H., 2003, Mapping from ASTER stereo image data: DEM validation and accuracy assessment: *International Society for Photogrammetry and Remote Sensing, Journal of Photogrammetry and Remote Sensing*, v. 57, p. 356–370, doi: 10.1016/S0924-2716(02)00164-8.
- Hovius, N., and Allen, M.B., 2000, Uplift and erosion of the eastern Greater Caucasus, Azerbaijan: The importance of orographic precipitation: *Eos (Transactions, American Geophysical Union)*, v. 81, no. 48, p. 1166.
- Inan, S., Yalcin, M.N., Guliev, I., Kuliev, K., and Feizullayev, A.A., 1997, Deep petroleum occurrences in the Lower Kura Depression, South Caspian Basin, Azerbaijan: An organic geochemical and basin modeling study: *Marine and Petroleum Geology*, v. 14, no. 7/8, p. 731–762, doi: 10.1016/S0264-8172(97)00058-5.
- Jackson, J., 1992, Partitioning of strike-slip convergent motion between Eurasia and Arabia in eastern Turkey and the Caucasus: *Journal of Geophysical Research*, v. 97, p. 12,471–12,479, doi: 10.1029/92JB00944.
- Jackson, J., and Ambraseys, N.N., 1997, Convergence between Eurasia and Arabia in eastern Turkey and the Caucasus, in Giardini, D., and Balassanian, S., eds., *Historical and prehistorical earthquakes in the Caucasus*: Kluwer Academic Publishers, p. 79–90.
- Jackson, J., and McKenzie, D., 1984, Active tectonics of the Alpine-Himalayan Belt between western Turkey and Pakistan: *Geophysical Journal of the Royal Astronomical Society*, v. 77, p. 185–264.
- Jackson, J., Norris, R., and Youngson, J., 1996, The structural evolution of active fault and fold systems in central Otago, New Zealand: Evidence revealed by drainage patterns: *Journal of Structural Geology*, v. 18, no. 2/3, p. 217–234, doi: 10.1016/S0191-8141(96)80046-0.
- Jackson, J., Priestly, K., Allen, M.B., and Berberian, M., 2002, Active tectonics of the South Caspian Basin: *Geophysical Journal International*, v. 148, p. 214–245, doi: 10.1046/j.1365-246X.2002.01588.x.
- Jarvis, A., Reuter, H.I., Nelson, A., and Guevara, E., 2006, Hole-filled seamless SRTM data, version 3: *International Center for Tropical Agriculture (CIAT)*.
- Jones, R.W., and Simmons, M., 1996, A review of the stratigraphy of Eastern Paratethys (Oligocene-Holocene): *Bulletin of the Natural History Museum of London*, v. 52, no. 1, p. 25–49.
- Keller, E.A., Gurrrola, L., and Tierney, T.E., 1999, Geomorphic criteria to determine direction of lateral propagation of reverse faulting and folding: *Geology*, v. 27, no. 6, p. 515–518, doi: 10.1130/0091-7613(1999)027<0515:GCTDDO>2.3.CO;2.
- Keskin, M., 2003, Magma generation by slab steepening and breakout beneath a subduction-accretion complex: An alternative model for collision-related volcanism in Eastern Anatolia, Turkey: *Geophysical Research Letters*, v. 30, no. 24, 8046, doi: 10.1029/2003GL018019.
- Khain, V.Y., 1975, Structure and main stages in the tectono-magmatic development of the Caucasus: An attempt at geodynamic interpretation: *American Journal of Science*, v. 275 A, p. 131–156.
- Kocyiğit, A., Yilmaz, A., Adamia, S., and Kuloshvili, S., 2001, Neotectonics of East Anatolia Plateau (Turkey) and Lesser Caucasus: Implication for transition from thrusting to strike-slip faulting: *Geodinamica Acta*, v. 14, p. 177–195, doi: 10.1016/S0985-3111(00)01064-0.
- Kopp, M.L., and Shcherba, I.G., 1985, Late alpine development of the east Caucasus: *Geotectonics*, v. 19, no. 6, p. 497–507.
- Král, J., and Gurbanov, A.G., 1996, Apatite fission track data from the Greater Caucasus pre-Alpine basement: *Chemie der Erde*, v. 56, p. 177–192.
- Kremenetskiy, A.A., Lapidus, A.V., and Voronovskiy, S.N., 1990, New data on the age and oil and gas potential of the basement of Kura depression, based on ultra-deep well logs: *Doklady of the National Academy of Sciences of the Union of Soviet Socialist Republics*, v. 312, no. 1–6, p. 139–142.
- Lozar, F., and Polino, R., 1997, Early Cenozoic uprising of the Greater Caucasus revealed by reworked calcareous nanofossils: *Terra Nova*, v. 9, p. 141.
- Lydolph, P.E., 1977, *Climates of the Soviet Union, world survey of climatology*: Amsterdam-Oxford-New York, Elsevier Scientific Publishing Company.
- Mangino, S., and Priestly, K., 1998, The crustal structure of the Southern Caspian region: *Geophysical Journal International*, v. 133, p. 630–648, doi: 10.1046/j.1365-246X.1998.00520.x.
- McClusky, S., Balassanian, S., Barka, A., Demir, C., Ergintav, S., Georgiev, I., Gurkan, O., Hamburger, M., Hurst, K., Kahle, H., Kastens, K., Kekelidze, G., King, R., Kotzev, V., Lenk, O., Mahmoud, S., Mishin, A., Nadariya, M., Ouzounis, A., Paradissis, D., Peter, Y., Prilepin, M., Reilinger, R., Sanli, I., Seeger, H., Tealeb, A., Toksoz, M.N., and Veis, G., 2000, Global positioning system constraints on plate kinematics and dynamics in the eastern Mediterranean and Caucasus: *Journal of Geophysical Research*, v. 205, no. B3, p. 5695–5719.
- McKenzie, D., 1972, Active tectonics of the Mediterranean region: *Geophysical Journal of the Royal Astronomical Society*, v. 30, p. 109–185.
- McQuarrie, N., Stock, J.M., Verdel, C., and Wernicke, B.P., 2003, Cenozoic evolution of Neotethys and implications for the causes of plate motions: *Geophysical Research Letters*, v. 30, no. 20, p. doi: 10.1029/2003GL017992.
- Meulenkamp, J.E., and Sissingh, W., 2003, Tertiary palaeogeography and tectonostratigraphic evolution of the northern and southern Peri-Tethys platforms and the intermediate domains of the African-Eurasian convergent plate boundary zone: *Palaeogeography, Palaeoclimatology, Palaeoecology*, v. 196, no. 1–2, p. 209–228, doi: 10.1016/S0031-0182(03)00319-5.
- Mitchell, J., and Westaway, R., 1999, Chronology of Neogene and Quaternary uplift and magmatism in the Caucasus, constraints from K-Ar dating of volcanism in Armenia: *Tectonophysics*, v. 304, p. 157–186, doi: 10.1016/S0040-1951(99)00027-X.
- Morton, A.C., Allen, M.B., Simmons, M., Spathopoulos, F., Still, J., Hinds, D.J., Ismail-Zadeh, A., and Kroonenberg, S.B., 2003, Provenance patterns in a neotectonic basin: Pliocene and Quaternary sediment supply to the South Caspian: *Basin Research*, v. 15, p. 321–337, doi: 10.1046/j.1365-2117.2003.00208.x.
- Murtuzayev, I., 2000, Implications of endogenous systems' tilting for tectonics of South Caspian Basin: *Basin Research*, 62nd European Association of Geoscientists and Engineers (EAGE) Conference and Technical Exhibition.
- Nadirov, R.S., Bagirov, E.B., Tagiyev, M.F., and Lerche, I., 1997, Flexural plate subsidence, sedimentation rates, and structural development of the super-deep South Caspian Basin: *Marine and Petroleum Geology*, v. 14, no. 4, p. 383–400, doi: 10.1016/S0264-8172(96)00054-2.
- Nalivkin, D.V., 1973, The Mediterranean geosyncline, in Nalivkin, D.V., ed., *Geology of the Union of Soviet Socialist Republics (English translation)*: Edinburgh, Oliver and Boyd, p. 578–685.
- Nalivkin, D.V., 1976, *Geologic map of the Caucasus (in Russian)*: Ministry of Geology, Union of Soviet Socialist Republics, scale 1:500,000.
- Oberlander, T.M., 1985, Origin of drainage transverse to structures in orogens, in Morisawa, M., and Hacker, J.T., eds., *15th Annual Binghamton Geomorphology Symposium*, p. 155–182.
- Oskin, M., and Iriondo, A., 2004, Large-magnitude transient strain accumulation on the Blackwater fault, Eastern California shear zone: *Geology*, v. 32, no. 4, p. 313–316, doi: 10.1130/G20223.1.
- Oskin, M., Perg, L., Blumentritt, D., Mukhopadhyay, S., and Iriondo, A., 2007, Slip rate of the Calico fault: Implications for geologic versus geodetic rate discrepancy in the Eastern California Shear Zone: *Journal of Geophysical Research*, v. 112, B03402, doi: 10.1029/2006JB004451.
- Philip, H., Cisternas, A., Gvishiani, A., and Gorshkov, A., 1989, The Caucasus: An actual example of the initial stages of continental collision: *Tectonophysics*, v. 161, p. 1–21, doi: 10.1016/0040-1951(89)90297-7.
- Philip, H., Rogozhin, E., Cisternas, A., Bousquet, J.C., Borisov, B., and Karakhanian, A., 1992, The Armenian earthquake of 1988 December 7: Faulting and folding, neotectonics and paleoseismicity: *Geophysical Journal International*, v. 110, p. 141–158, doi: 10.1111/j.1365-246X.1992.tb00718.x.
- Philip, H., Avagyan, A., Karakhanian, A., Ritz, J.-F., and Rebai, S., 2001, Estimating slip rates and recurrence intervals for strong earthquakes along an intracontinental fault: Example of the Pambak-Sevan-Sunik fault (Armenia): *Tectonophysics*, v. 343, p. 205–232, doi: 10.1016/S0040-1951(01)00258-X.
- Priestley, K., Baker, C., and Jackson, J., 1994, Implications of earthquake focal mechanism data for the active tectonics of the south Caspian Basin and surrounding regions: *Geophysical Journal International*, v. 118, p. 111–141, doi: 10.1111/j.1365-246X.1994.tb04679.x.
- Rebai, S., Philip, H., Dorbath, L., Borissoff, B., Haessler, H., and Cisternas, A., 1993, Active tectonics in the Lesser Caucasus: Coexistence of compressive and extensional structures: *Tectonics*, v. 12, no. 5, p. 1089–1114, doi: 10.1029/93TC00514.
- Reilinger, R., and Barka, A., 1997, GPS Constraints on fault slip rates in the Arabia-Africa-Eurasia Plate Collision Zone: Implications for earthquake recurrence times, in Giardini, D., and Balassanian, S., eds., *Historical and prehistorical earthquakes in the Caucasus*: Kluwer Academic Publishers, p. 91–108.
- Reilinger, R., McClusky, S., Souter, B.J., Hamburger, M., Prilepin, M., Mishin, A., Guseva, T., and Balassanian, S., 1997, Preliminary estimates of plate convergence in the Caucasus collision zone from global positioning

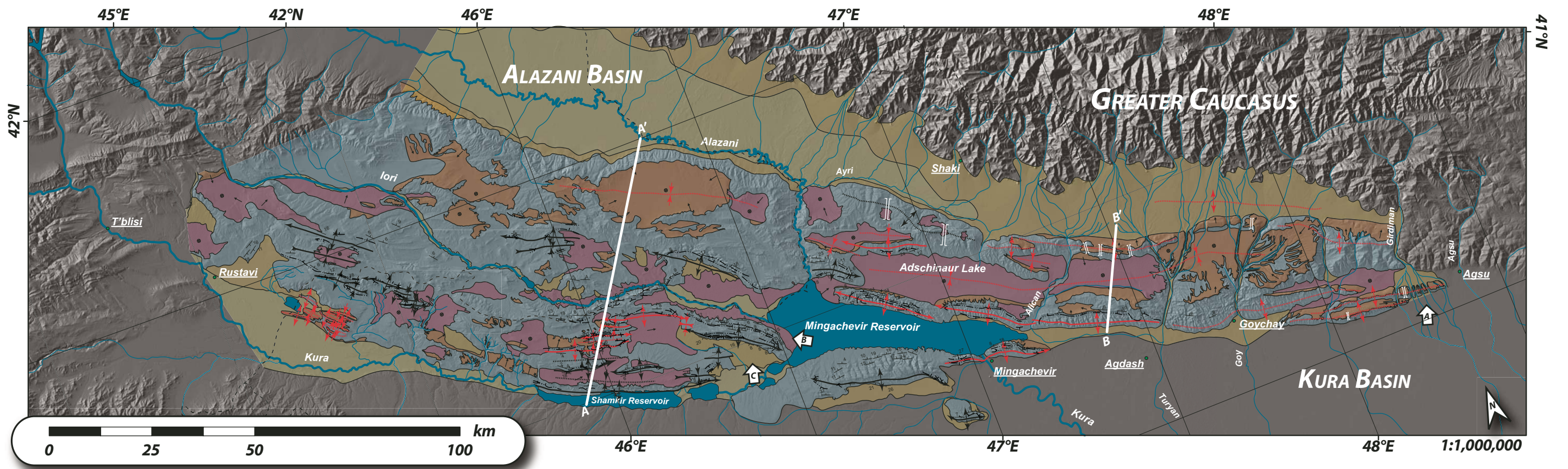
- system measurements: *Geophysical Research Letters*, v. 24, no. 14, p. 1815–1818.
- Reilinger, R., McClusky, S., and Lawrence, S., 2004, GPS constraints on continental deformation in the eastern Mediterranean and Caucasus Region: Evidence for plate/block-like behavior of the continental lithosphere: *Geophysical Research Abstracts*, v. 6, p. 04380.
- Reilinger, R., McClusky, S., Vernant, P., Lawrence, S., Ergintav, S., Cakmak, R., Ozener, H., Kadirov, F., Guliev, I., Stepanyan, R., Nadariya, M., Hahubia, G., Mahmoud, S., Sakr, K., ArRajehi, A., Paradissis, D., Al-Aydrus, A., Prilepin, M., Guseva, T., Evren, E., Dmitrova, A., Filikov, S. V., Gomez, F., Al-Ghazzi, R., and Karam, G., 2006, GPS constraints on continental deformation in the Africa-Arabia-Eurasia continental collision zone and implications for the dynamics of plate interactions: *Journal of Geophysical Research*, v. 111, B05411, doi: 10.1029/2005JB004051.
- Robertson, A.H.F., 2000, Mesozoic-Tertiary tectonic-sedimentary evolution of the south Tethyan oceanic basin and its margins in southern Turkey, in Bozkurt, E., Winchester, J.A., and Piper, J.D.A., eds., *Tectonics and magmatism in Turkey and the surrounding area: The Geological Society of London Special Publication*, p. 97–138.
- Robinson, A.G., Banks, C.J., Rutherford, M.M., and Hirst, J.P.P., 1995, Stratigraphic and structural development of the Eastern Pontides, Turkey: *The Geological Society of London*, v. 152, p. 861–872, doi: 10.1144/gsjgs.152.5.0861.
- Saintot, A., and Angelier, J., 2002, Tectonic paleostress fields and structural evolution on the NW-Caucasus fold-and-thrust belt from Late Cretaceous to Quaternary: *Tectonophysics*, v. 357, p. 1–31, doi: 10.1016/S0040-1951(02)00360-8.
- Saroglu, F., 1992, Active fault map of Turkey: General Directorate of Mineral Research and Exploration (MTA).
- Sella, G. F., Dixon, T. H., and Mao, A., 2002, REVEL: A model for Recent plate velocities from space geodesy: *Journal of Geophysical Research*, v. 107, no. B4, p. 2081, doi: 10.1029/2000JB000033.
- Şengör, A.M.C., Özeren, S., Genç, T., and Zor, E., 2003, East Anatolian high plateau as a mantle-supported, north-south shortened domal structure: *Geophysical Research Letters*, v. 30, no. 24, 8045, doi: 10.1029/2003GL017858.
- Sobornov, K.O., 1994, Structure and petroleum potential of the Dagestan thrust belt, northeastern Caucasus, Russia: *Bulletin of Canadian Petroleum Geology*, v. 42, no. 3, p. 352–364.
- Suppe, J., 1983, Geometry and kinematics of fault-bend folding: *American Journal of Science*, v. 283, p. 684–721.
- Suppe, J., and Medwedeff, D.A., 1990, Geometry and kinematics of fault-propagation folding: *Eclogae Geologicae Helvetiae*, v. 83, no. 3, p. 409–454.
- Tagiyev, R.E., 1984, New data on the structure of the Kura Basin and the southeasterly plunge of the Greater Caucasus: *Geotectonics*, v. 18, no. 5, p. 444–447.
- Talebian, M., and Jackson, J., 2002, Offset on the main Recent fault of NW Iran and implications for the late Cenozoic tectonics of the Arabia-Eurasia collision zone: *Geophysical Journal International*, v. 150, p. 422–439, doi: 10.1046/j.1365-246X.2002.01711.x.
- Tan, O., and Taymaz, T., 2006, Active tectonics of the Caucasus: Earthquake source mechanisms and rupture histories obtained from inversion of teleseismic body waveforms, in Dilek, Y., and Pavlides, S., eds., *Postcollisional tectonics and magmatism of the Mediterranean region and Asia: Geological Society of America Special Paper*, p. 531–578.
- Tevelev, A.V., and Blyumkin, E.I., 1990, Comparative tectonics from space images of the Kura and Surkhanda'y'a depressions: *Soviet Journal of Remote Sensing*, v. 7, no. 3, p. 509–516.
- Thatcher, W., 2007, Microplate model for the present-day deformation of Tibet: *Journal of Geophysical Research*, v. 112, B01401, doi: 10.1029/2005JB004244.
- Triep, E.G., Abers, G.A., Lerner-Lam, A.L., Mishatkin, V., Zakharchenko, N., and Starovoi, O., 1995, Active thrust front of the Greater Caucasus: The April 29, 1991, Racha earthquake sequence and its tectonic implications: *Journal of Geophysical Research*, v. 100, no. B3, p. 4011–4033, doi: 10.1029/94JB02597.
- Vasiliev, I., Krijgsman, W., Langereis, C.G., Panaiotu, C.E., Matenco, L., and Bertotti, G., 2004, Towards an astrochronological framework for the eastern Paratethys Mio-Pliocene sedimentary sequences of the Foscani basin (Romania): *Earth and Planetary Science Letters*, v. 227, p. 231–247, doi: 10.1016/j.epsl.2004.09.012.
- Vernant, P., Nilforoushan, F., Hatzfeld, D., Abbassi, M.R., Vigny, C., Masson, F., Nankali, H., Martinod, J., Ashtiani, A., Bayer, R., Tavakoli, F., and Chery, J., 2004, Present-day crustal deformation and plate kinematics in the Middle East constrained by GPS measurements in Iran and northern Oman: *Geophysical Journal International*, v. 157, p. 381–398, doi: 10.1111/j.1365-246X.2004.02222.x.
- Vincent, S.J., Morton, A.C., Carter, A., Gibbs, S., and Teimuraz, G.B., 2007, Oligocene uplift of the Western Greater Caucasus: An effect of initial Arabia-Eurasia collision: *Terra Nova*, v. 19, p. 160–166, doi: 10.1111/j.1365-3121.2007.00731.x.
- Wells, S.G., Bullard, T.F., Menges, C.M., Drake, P.G., Karas, P.A., Kelson, K.L., Ritter, J.B., and Wesling, J.R., 1988, Regional variations in tectonic geomorphology along a segmented convergent plate boundary pacific coast of Costa Rica: *Geomorphology*, v. 1, p. 239–265, doi: 10.1016/0169-555X(88)90016-5.
- Wessel, R., and Smith, W.H.F., 1995, New version of the generic mapping tools released: *Eos (Transactions, American Geophysical Union)*, v. 76, p. 329, doi: 10.1029/95EO00198.
- Westaway, R., 1990, Seismicity and tectonic deformation rate in Soviet Armenia: Implications for local earthquake hazard and evolution of adjacent regions: *Tectonics*, v. 9, no. 3, p. 477–503, doi: 10.1029/TC009i003p00477.
- Westaway, R., 1994, Present-day kinematics of the Middle East and eastern Mediterranean: *Journal of Geophysical Research*, v. 99, no. B6, p. 12,071–12,090, doi: 10.1029/94JB00335.
- Woodward, N.B., Boyer, S.E., and Suppe, J., 1989, Balanced geological cross sections: An essential technique in geological research and exploration: Washington, D.C., *Short Courses in Geology*, American Geophysical Union, 132 p.
- Yamaguchi, Y., Kahle, A.B., Tsu, H., Kawakami, T., and Pniel, M., 1998, Overview of advanced spaceborne thermal emission and reflection radiometer (ASTER): *IEEE Transactions on Geoscience and Remote Sensing*, v. 36, no. 4, p. 1062–1071, doi: 10.1109/36.700991.
- Yılmaz, A., Adamia, S., Chabukiani, A., Chkhotua, T., Erdogan, K., Tuzcu, S., and Karabiyikoglu, M., 2000, Structural correlation of the southern Transcaucasus (Georgia)-eastern Pontides (Turkey), in Bozkurt, E., Winchester, J.A., and Piper, J.D.A., eds., *Tectonics and magmatism in Turkey and the surrounding area: The Geological Society of London Special Publication*, p. 171–182.
- Zonenshain, L.P., and Le Pichon, X., 1986, Deep basins of the Black Sea and Caspian Sea as remnants of Mesozoic back-arc basins: *Tectonophysics*, v. 123, p. 181–211, doi: 10.1016/0040-1951(86)90197-6.

MANUSCRIPT RECEIVED 15 MAY 2008

REVISED MANUSCRIPT RECEIVED 29 JANUARY 2009

MANUSCRIPT ACCEPTED 7 MARCH 2009

Printed in the USA



Geomorphic surfaces

- ACTIVE SURFACE** - Active surfaces, either alluvial fans (A) or floodplains (F).
- ABANDONED SURFACE** - Smooth inactive surface that can be documented as a relict Quaternary surface. A surface lacking a clear sediment source and is not a resistant unit.
- QUERIED SURFACE** - Smooth surface of questionable origins. Occurring both in deposition sites (valleys) and on hillslopes. Valley bottoms could be Quaternary surfaces or exposures of bedrock. Flat hill slopes that cannot be clearly documented as relict Quaternary surfaces.
- INCISED SURFACE** - Heavily incised areas. Surfaces may be exposures of pre-Quaternary bedrock or incised areas of Quaternary surfaces.

- Horizontal surface
- Gentle slope
- Moderate slope
- Steep slope
- Wind gap
- Viewpoints for RIMS screenshots in Figure 2

Bedrock symbols

- ACTIVE STRUCTURES** (Deforms relict or active geomorphic surfaces)
- ACTIVE PLUNGING ANTICLINE**
 - ACTIVE ANTICLINE**
 - ACTIVE PLUNGING SYNCLINE**
 - ACTIVE SYNCLINE**
 - ACTIVE PLUNGING ANTICLINE (INFERRED)**
 - ACTIVE ANTICLINE (INFERRED)**
 - ACTIVE PLUNGING SYNCLINE (INFERRED)**
 - ACTIVE SYNCLINE (INFERRED)**
- INACTIVE STRUCTURES** (Only deforms bedrock or queried surfaces)
- PLUNGING ANTICLINE**
 - ANTICLINE**
 - PLUNGING SYNCLINE**
 - SYNCLINE**
 - PLUNGING ANTICLINE (INFERRED)**
 - ANTICLINE (INFERRED)**
 - PLUNGING SYNCLINE (INFERRED)**
 - SYNCLINE (INFERRED)**
- ¹² Strike and dip of isolated marker bed measured in RIMS
- Marker bed (tick indicates dip direction)

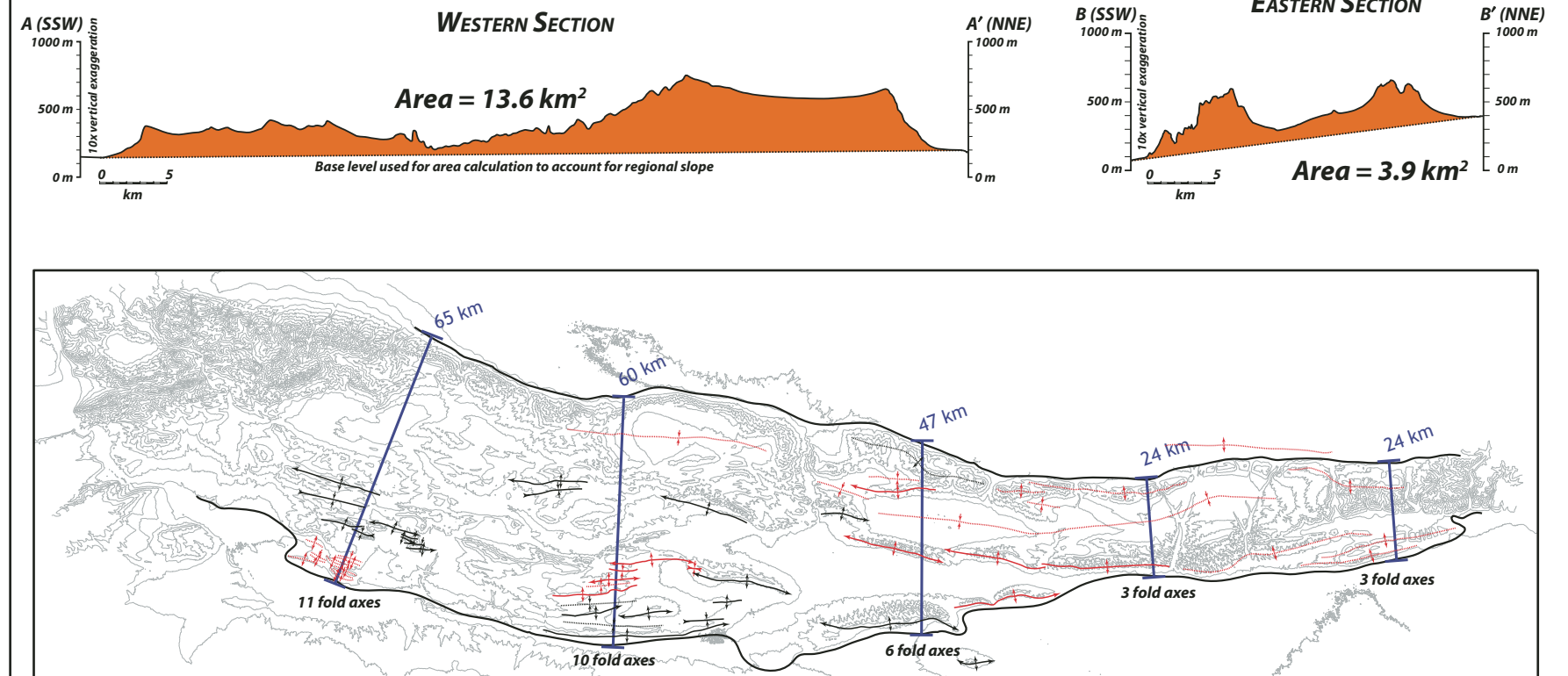
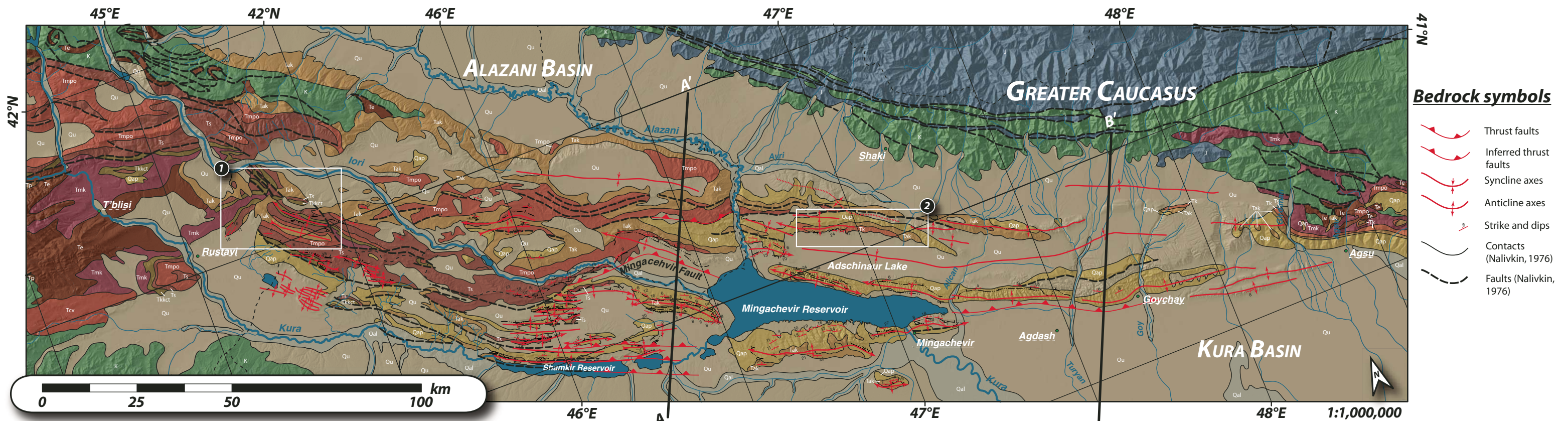
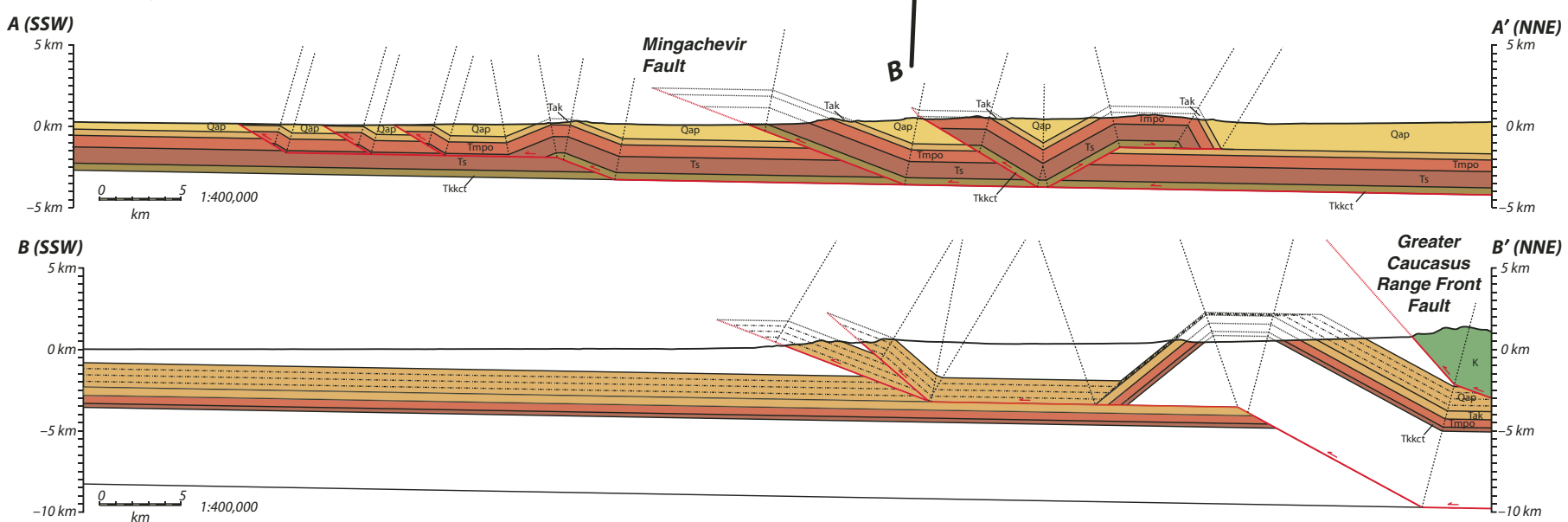
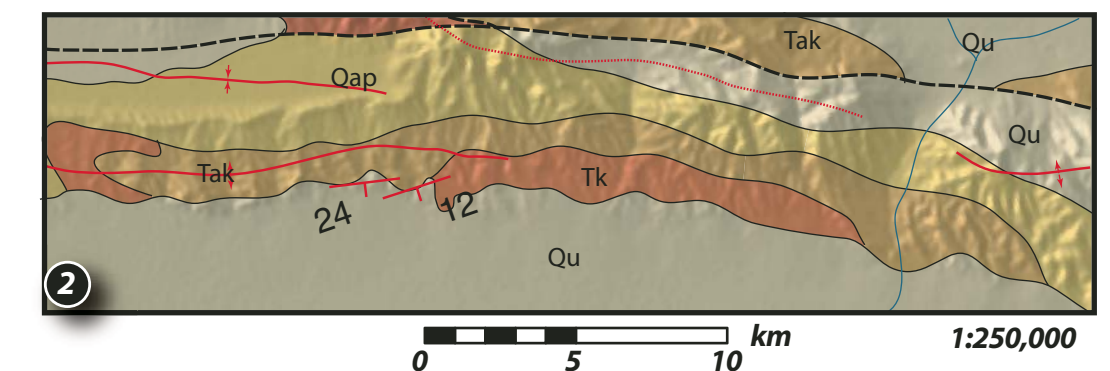
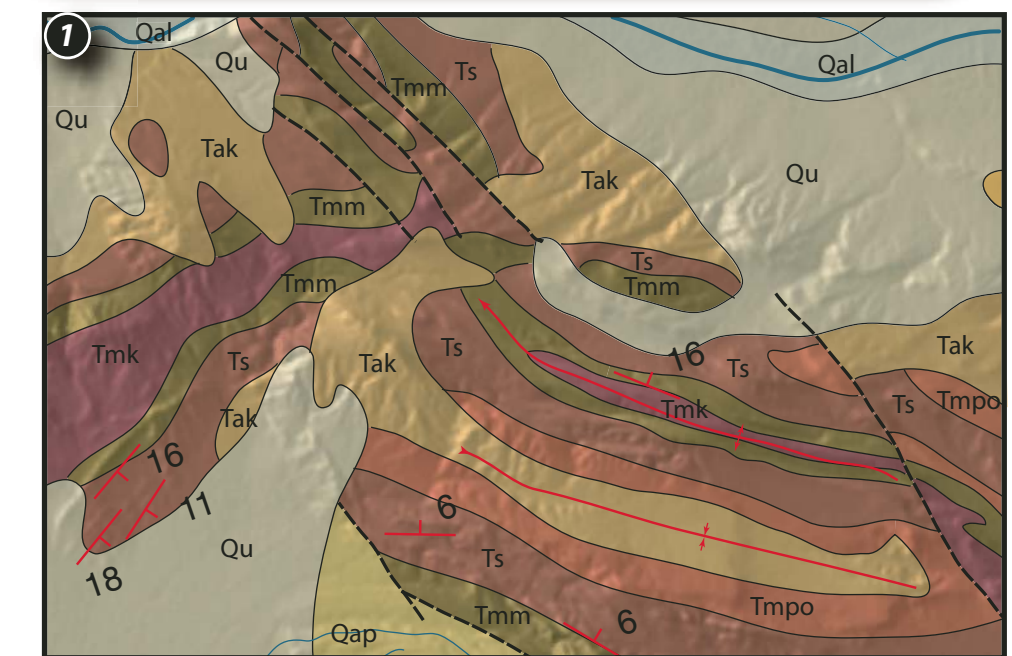


Plate 1. New neotectonic map of the Kura fold-thrust belt compiled from observations made from analysis of both Advanced Spaceborne Thermal Emission and Reflection Radiometer (ASTER) and Shuttle Radar Topographic Mission (SRTM) data and mapped using Real-Time Interactive Mapping System (RIMS). Base hillshade image generated from SRTM 90-m digital elevation model (DEM). See text for discussion. Panels in lower-right corner show topographic data. Upper panels show topographic profiles at 10× vertical exaggeration, and indicate that the cross-sectional area of topography elevated above a baseline connecting the floors of the Kura and Alazani basins decreases eastward, such that the area of western section is ~3.5 times that to the east. Lower panel shows simplified topographic map. Undecorated black lines show margins of the Kura fold-thrust belt, which is also delineated by topographic contours in gray (100-m interval). Blue lines bracket cross-strike width of topography. Decorated red and black lines show axial traces of active and inactive folds, respectively. Note the systematic eastward decrease in both topographic width and structural complexity.



- Bedrock symbols**
- Thrust faults
 - Inferred thrust faults
 - Syncline axes
 - Anticline axes
 - Strike and dips
 - Contacts (Nalivkin, 1976)
 - Faults (Nalivkin, 1976)



Map Units (Nalivkin, 1976)

<table border="0"> <tr><td>Qal</td><td>MODERN ALLUVIAL SEDIMENTS- Coarse gravel, sand, clay, calcareous, tuff/tuffaceous.</td></tr> <tr><td>Qu</td><td>UNDIFFERENTIATED QUATERNARY</td></tr> <tr><td>Qap</td><td>APSHERON STAGE- Sand, clay, loam, sandstone, coarse gravel, conglomerate, liparite tuffs.</td></tr> <tr><td>Tak</td><td>AKCHAGYL STAGE- Clay, sand, sandstone, loam, conglomerate, volcanic ash.</td></tr> <tr><td>Tk</td><td>KIMMERIAN STAGE- Sand, clay, sandstone, conglomerate.</td></tr> </table>	Qal	MODERN ALLUVIAL SEDIMENTS - Coarse gravel, sand, clay, calcareous, tuff/tuffaceous.	Qu	UNDIFFERENTIATED QUATERNARY	Qap	APSHERON STAGE - Sand, clay, loam, sandstone, coarse gravel, conglomerate, liparite tuffs.	Tak	AKCHAGYL STAGE - Clay, sand, sandstone, loam, conglomerate, volcanic ash.	Tk	KIMMERIAN STAGE - Sand, clay, sandstone, conglomerate.	<table border="0"> <tr><td>Tmpo</td><td>MAEOTIAN AND PONTIAN STAGES- Shells, clay, sand, marl, sandstone, conglomerate.</td></tr> <tr><td>Ts</td><td>SARMATIAN STAGE- Clay, sandstone, marl, calcarenite, siltstone, shells, conglomerate, tuffaceous sandstones, coal, tuff, crusty and rhyolitic dacite.</td></tr> <tr><td>Tkkct</td><td>KONKIAN, KARAGANIAN, CHOKRAKIAN, TARKHANIAN- Clay, sand, sandstone, calcarenite, marl, coarse gravel, conglomerate</td></tr> <tr><td>Tct</td><td>CHOKRAKIAN AND TARKHANIAN STAGE- Clay, sand, sandstone, shells.</td></tr> <tr><td>Tmk</td><td>MAYKOPIAN STAGE- Clay, sand, sandstone, marl.</td></tr> </table>	Tmpo	MAEOTIAN AND PONTIAN STAGES - Shells, clay, sand, marl, sandstone, conglomerate.	Ts	SARMATIAN STAGE - Clay, sandstone, marl, calcarenite, siltstone, shells, conglomerate, tuffaceous sandstones, coal, tuff, crusty and rhyolitic dacite.	Tkkct	KONKIAN, KARAGANIAN, CHOKRAKIAN, TARKHANIAN - Clay, sand, sandstone, calcarenite, marl, coarse gravel, conglomerate	Tct	CHOKRAKIAN AND TARKHANIAN STAGE - Clay, sand, sandstone, shells.	Tmk	MAYKOPIAN STAGE - Clay, sand, sandstone, marl.	<table border="0"> <tr><td>Te</td><td>UNDIFFERENTIATED EOCENE SEDIMENTS- Marl, clay, conglomerate, sandstone, siltstone, limestone, rhyolite, andesite, dacite, tuff, basalts.</td></tr> <tr><td>Tp</td><td>UNDIFFERENTIATED PALEOCENE- Clay, sandstone, marl, limestone, conglomerate, dacites, tuffs.</td></tr> <tr><td>Tcv</td><td>UNDIFFERENTIATED CENOZOIC VOLCANICS</td></tr> <tr><td>K</td><td>UNDIFFERENTIATED CRETACEOUS</td></tr> <tr><td>J</td><td>UNDIFFERENTIATED JURASSIC</td></tr> </table>	Te	UNDIFFERENTIATED EOCENE SEDIMENTS - Marl, clay, conglomerate, sandstone, siltstone, limestone, rhyolite, andesite, dacite, tuff, basalts.	Tp	UNDIFFERENTIATED PALEOCENE - Clay, sandstone, marl, limestone, conglomerate, dacites, tuffs.	Tcv	UNDIFFERENTIATED CENOZOIC VOLCANICS	K	UNDIFFERENTIATED CRETACEOUS	J	UNDIFFERENTIATED JURASSIC
Qal	MODERN ALLUVIAL SEDIMENTS - Coarse gravel, sand, clay, calcareous, tuff/tuffaceous.																															
Qu	UNDIFFERENTIATED QUATERNARY																															
Qap	APSHERON STAGE - Sand, clay, loam, sandstone, coarse gravel, conglomerate, liparite tuffs.																															
Tak	AKCHAGYL STAGE - Clay, sand, sandstone, loam, conglomerate, volcanic ash.																															
Tk	KIMMERIAN STAGE - Sand, clay, sandstone, conglomerate.																															
Tmpo	MAEOTIAN AND PONTIAN STAGES - Shells, clay, sand, marl, sandstone, conglomerate.																															
Ts	SARMATIAN STAGE - Clay, sandstone, marl, calcarenite, siltstone, shells, conglomerate, tuffaceous sandstones, coal, tuff, crusty and rhyolitic dacite.																															
Tkkct	KONKIAN, KARAGANIAN, CHOKRAKIAN, TARKHANIAN - Clay, sand, sandstone, calcarenite, marl, coarse gravel, conglomerate																															
Tct	CHOKRAKIAN AND TARKHANIAN STAGE - Clay, sand, sandstone, shells.																															
Tmk	MAYKOPIAN STAGE - Clay, sand, sandstone, marl.																															
Te	UNDIFFERENTIATED EOCENE SEDIMENTS - Marl, clay, conglomerate, sandstone, siltstone, limestone, rhyolite, andesite, dacite, tuff, basalts.																															
Tp	UNDIFFERENTIATED PALEOCENE - Clay, sandstone, marl, limestone, conglomerate, dacites, tuffs.																															
Tcv	UNDIFFERENTIATED CENOZOIC VOLCANICS																															
K	UNDIFFERENTIATED CRETACEOUS																															
J	UNDIFFERENTIATED JURASSIC																															

Plate 2. New geologic map compiled by integrating neotectonic observations from the present study with previously published geologic mapping (Nalivkin, 1976). The original map illustrated faults (heavy black dashed lines) but did not indicate fold axes or fault type. Symbols in red are from our new neotectonic mapping. Faults were added only along the two lines of section, with the exception of the Mingachevir fault, which was extended based on previous mapping (Agabekov et al., 1971; Berberian and King, 1997). When constructing the cross sections, we interpreted the faults on Nalivkin's map as south-directed thrusts, based on the predominance of south-verging folds in the region. Geologic cross sections in lower-right corner are reproduced from Figures 8 and 9, in which they are also reconstructed. Two enlargements of key areas appear on the lower-left corner. Enlargement 1 highlights the syntectonic nature of the upper Pliocene Akchagyl sediments at the western end of the fold-thrust belt. The Akchagyl in this area appears to crosscut underlying folded strata but is also deformed, suggesting it was deposited during the growth of the folds. In stark contrast, Akchagyl sediments in the eastern portion of the fold-thrust belt appear to be concordant with folds in underlying units as highlighted in enlargement 2.